INVESTIGATION OF COASTAL FLOOD PROBLEM IN IZMIR BAY

A Thesis Submitted to
the Graduate School of Engineering and Science of
İzmir Institute of Technology
in Partial Fulfillment of the Requirement for the Degree of

MASTER OF SCIENCE

in Civil Engineering

by
Salih AK

July 2021
İZMİR

ACKNOWLEDGEMENT

I would like to thank my esteemed advisor, Associate Professor Dr. Bergüzar Özbahçeci, who made me like and taught the field of Coastal Engineering and shared her knowledge and experience during my thesis studies.

I would like to thank Izmir Metropolitan Municipality for sharing the meteorological data with me.

I would like to thank Dr. Gökhan Kaboğlu for sharing the Bay of İzmir bathymetry data with me.

My thanks also go to the European Centre for Medium-Range Weather Forecasts (ECMWF) for providing ERA-5 wind data.

I would like to thank Kerem Güner for his valuable friendship and for being with me.

I would like to thank my family: my father Mustafa Ak, my sister Tuğçe Angış, my aunt Fatma Küçük for supporting me throughout my life.

Last but not least, I would like to thank my precious grandmother Elmas Ak, who raised me and was the biggest supporter in my life.

ABSTRACT

INVESTIGATION OF COASTAL FLOOD PROBLEM IN IZMIR BAY

Izmir, with its long coastline, is one of Turkey's leading tourism and trade cities. The coastal flood is an important problem in İzmir Bay. The literature review shows that there is no study that covers all the elements of the problem such as wind and wave climate, fluctuations in the sea level and coastal flood calculations in İzmir Bay.

In this study, the ERA5 wind dataset developed by the European Center for Medium Range Weather Forecasts was used to determine extreme wind speeds. The data were verified using in-situ wind measurements data. Then, the fluctuations in sea water level caused by astronomic and atmospheric effects such as tides, wind and wave set-up and barometric effects were examined by the analysis of sea water level measurement data of the Izmir Metropolitan Municipality in Bostanlı and Pasaport and the tide gauge station data of the General Directorate of Mapping in Mentes. The long-term trend of sea level was examined using Theil-Sen and the line of best-fit methods. Then, the reliability of the trends was demonstrated by performing the Mann-Kendal test. Calculated extreme wind speeds and sea level fluctuations were taken into account to estimate the waves in front of coastal protection structures using a wave model called SWAN. Then, in order to predict the coastal flood amounts, the wave overtopping was calculated by the artificial neural network method. It is concluded that the most sensitive places in İzmir Bay in terms of coastal floods are the areas protected by vertical walls.

ÖZET

İZMİR KÖRFEZİNDE KIYI TAŞKIN SORUNUNUN ARAŞTIRILMASI

İzmir, uzun sahil şeridi ile Türkiye'nin önde gelen turizm ve ticaret şehirlerinden biridir. Özellikle İzmir körfezi yoğun bir kullanıma sahiptir. İzmir körfezinde son yıllarda sıklığı artan bir şekilde deniz taşkınları meydana geldiği ve deniz taşkınları sırasında büyük miktarda deniz suyunun arkadaki kara alanına taştığı, trafik sorunlarına neden olduğu, binalara ve dinlenme tesislerine zarar verdiği gözlemlenmiştir. Literatür araştırması, rüzgar iklimi, deniz seviyesindeki değişimler, dalga iklimi ve deniz taşkın hesaplamaları gibi sorunun tüm unsurlarını içeren ve İzmir körfezindeki deniz taşkın sorununu bütünsel olarak araştıran bir çalışmanın olmadığını göstermektedir.

Bu çalışmada, ekstrem rüzgar hızlarını belirlemek için Avrupa Orta Menzilli Hava Tahminleri Merkezi'nin (ECMWF) geliştirdiği ERA5 rüzgar veri seti kullanılmıştır. Veriler, İzmir Büyükşehir Belediyesi'nin yerinde rüzgar ölçümleri kullanılarak doğrulanmıştır. Ardından gelgit, rüzgar ve dalga kabarması, barometric kabarma gibi astronomik ve atmosferik etkiler ile oluşan deniz suyu seviyesindeki değişimler, İzmir Büyükşehir Belediyesi'nin Bostanlı ve Pasaport'taki deniz suyu seviyesi ölçüm verileri ve Harita Genel Müdürlüğü'nün Mentes'teki mareograf istasyonu verilerinin analizi ile incelenmiştir. 21 yıllık Mentes verileriyle, Theil-Sen ve "en iyi uyan doğru" yöntemleri kullanılarak deniz seviyesinin uzun dönemde artış eğilimi incelenmiştir. Daha sonra Mann-Kendal testi yapılarak artış eğilimlerinin güvenirliliği gösterilmiştir. Hesaplanan ekstrem rüzgar hızları ve deniz seviyesindeki artış dikkate alınarak, kıyı koruma yapılarının önündeki dalgalar, SWAN adı verilen bir dalga modeli kullanılarak tahmin edilmiştir. Daha sonra deniz taşkın miktarlarını tahmin edebilmek için yapay sinir ağları yöntemi ile dalga aşması hesaplanmıştır. İzmir körfezinde deniz taşkınları açısından en hassas yerlerin dik duvarla korunan bölgeler olduğu sonucuna varılmıştır.

TABLE OF CONTENTS

LIST OF FIGURES

Figure **Page**

Figure **Page**

LIST OF TABLES

CHAPTER 1

INTRODUCTION

1.1 Research Background and Problem Statement

Izmir is situated around the protected Izmir Bay on the Aegean Sea's heavily indented shore. Izmir has the second biggest port and it is the third largest city in Turkey. Izmir, with its extensive coastline, is one of the country's key tourist and commercial centers. Izmir coastline, which attracts attention for its natural, cultural, and historical treasures, is heavily utilized. Izmir Inner Bay refers to the coastline between the old Dalyan in Cigli to the north and Balcova to the south. The inner bay is surrounded by restaurants, cafés, and entertainment venues that are densely inhabited and it is very attractive for domestic and international visitors. In addition, Izmir's inner bay is bordered by a continuous coastal road.

The balance between structural areas and green spaces has worsened as a result of increased urbanization, industrialization, and population density growth. The two photos in Figure 2.1, obtained in 1984 and 2015, illustrate the changes that have occurred in the urban area and along the shore over the given time period.

Figure 1.1. Two images of İzmir Bay captured in 1984 (top) and in 2015 (bottom)

Figure 1.1 demonstrates that Izmir's shoreline and coastal area have been constantly enlarged through land reclamation. This expansion through filling has damaged the natural stability of the seabed's topography and increased the coast's susceptibility to the impacts of coastal flooding.

Izmir is resonant with sea and wind. In the summer, the cooling sea air dispels the scorching heat of the sun. When the wind is high, however, it causes waves accompanied by a storm surge, which raises the water level of the Bay. Coastal flooding occurs due to the combination of wind and waves and an increase in water level, which results in waves overtopping on the coastal protection systems. Along the coast, there are traditional coastal protection structures, such as sloping-type coastal revetments and vertical walls constructed parallel to the coast to protect the people, nearby roads, and buildings from coastal flooding and catastrophic sea effects. During a recent coastal flood, it was noted that a massive quantity of sea water inundated the reclaimed area, causing traffic problems and damage to structures and recreational amenities. The images in Figure 1.2 were captured during a recent coastal flood disaster in the city center of Izmir.

Figure 1.2. Example photos showing the consequences of coastal flood hazard events in the Izmir city center

The coastal flood events of the last 10 years, together with dates and the affected regions, are tabulated in Table 1.1.

Table 1.1. Coastal flood events of the last 10 years together with date sand affected areas

Date	Affected Areas
04.12.2012	KORDON-ALSANCAK
21.09.2015	CUMHURIYET SQUARES, KONAK
18.01.2018	ALSANCAK, KORDON
23.12.2019	KARSIYAKA
05.02.2020	KARSIYAKA,1. KORDON, GUNDOGDUAND CUMHURIYET SQUARES
14.12.2020	MAVISEHIR
08.02.2021	KARSIYAKA
29-30.11.2021	KARSIYAKA

The frequency of coastal flood events is rising, as seen in Table 1.1. This rise in Izmir Bay may be due to climate change caused by global warming. In recent years, the sea-level rise and extremeness of atmospheric and marine conditions caused by climate change have become evident. Rising sea levels, storm surges, and high waves are external influences affecting coastal defense structures that are impacted by climate change. Damage to coastal infrastructure, coastal erosion, morphological change, and coastal flood disasters are anticipated to increase as a result of sea level rise and the extreme wind and wave regimes. Consequently, research on the evaluation of coastal hazards, accompanied by changes in atmospheric and ocean conditions owing to climate change, has become crucial and should be conducted. A literature survey shows that there is not a complementary study to investigate the coastal flood problem in Izmir Bay including all elements of the problem such as the wind climate, sea level fluctuations, wave climate, and coastal flood calculations.

1.2. Aim and Scope of the Study

This study aims to investigate the coastal flood hazard problem in the inner bay of İzmir in detail. The main objectives are:

1- To determine the wind climate and extreme values of the wind speed in Izmir Bay

2- To examine the sea level fluctuations in Izmir Bay considering the tides, astronomic effects (wind and wave set-up, barometric and coriolis effects) and estimation of sea level increase trend due to climate change

3- To estimate the wave climate by numerical modeling and determine the extreme waves in front of the coastal protection structures

4- To calculate the coastal flood amounts considering the wave overtopping at vertical wall and sloping type revetments that exist in Izmir Bay.

1.3. The structure of the Thesis

The thesis is constructed as following: a review of previous studies is provided in Chapter 2. Data used are given in Chapter 3. In Chapter 4, wind climate studies are explained. Fluctuations in sea water level are examined in Chapter 5. In Chapter 6, modeling of waves and determination of wave parameters are explained. In Chapter 7, coastal flood calculations are given. Finally, conclusions are presented in Chapter 8.

CHAPTER 2

LITERATURE REVIEW

The combined effects of huge waves, storm surges, high tides, and mean sea level anomalies can result in exceptionally high water level events along the coast. The morphology of the coastal zone influences tides, storm surges, and waves in turn. All these contributing factors should be considered, including the impact of sea level rise on the likelihood of coastal flooding. Due to the unpredictable nature of coastal storms, nonlinear interactions of physical processes (such as tidal currents and waves), and changes in coastal geomorphology, the impact of sea level rise on episodic flooding events is difficult to predict. Currently only occasional high water events, such as the once-in-a-century flood, will occur more frequently as a result of sea level rise. It can vary greatly depending on where you are in the world, how much sea level rise affects this frequency. The interaction of the aforementioned factors, which vary from place to place, determines how much sea level rise will increase (hit) the frequency of occurrence of a given flood level (IPCC, 2012).

Demirkesen et al. (2007), in response to global climate change, the Intergovernmental Panel on Climate Change (IPCC) claims that global mean sea level rise (MSLR) has accelerated in the twentieth century. If this momentum continues, some coastal areas are likely to be flooded by 2100. For timely action to be taken, it is essential to be able to determine how differently different coastlines are vulnerable to future flood hazards due to global climate change. Therefore, a study was conducted to determine how much of the coastline areas of the Izmir region are at risk of flooding, using a digital elevation model (DEM) obtained by the shuttle's radar topography mission (SRTM). South İzmir, where the research area (6,107 km2) has 2.1 and 3.7 percent of the coastal areas that could be inundated with a rise of 2 and 5 m in local sea level until 2100, and which includes the southern coastline of İzmir Bay. They concluded that the shores of the Bay were found. The towns of Bornova, Konak, Balçova, Narlidere, Güzelbahce, Foca, Urla and Dikili generally seem less sensitive to estimated sea level rise than the coasts of İzmir Bay.

According to Karaca and Nicholls (2008), it is estimated that urbanization, which frequently occurs in coastal areas, will continue with the rapid increase in the urban

population, which was 14% of the total population in 1950. Intensive migration from the east and south of Turkey to major coastal cities such as Istanbul and Izmir is responsible for the increase in the urban population of Adana, Antalya and Alanya. As a result, the population at risk of sea level rise is likewise increasing. The majority of Turkish coasts appear to suffer from sea level fluctuations within the accepted sea level rise range (1-2 mm/year). While sea level rises significantly more than the global rise in many of the main river deltas, areas, where the rate of sea level rise is less than 1-2 mm/year (eg Samsun to Antalya), are considered to be tectonic. It includes a first-order assessment of the impacts of increased sea level rise and some other aspects of climate change on Turkey's coastal regions. It is estimated that there will be between 10 and 20 centimeters of sea level rise globally in the 20th century.

Ergin and Guler (2014) have been that the effects of climate change on the design and design parameters of coastal structures and the development of coastal cities along the Turkish coastline are investigated using two different case scenarios. It was concluded that the two features related to climate change that have the greatest impact on coastal areas are sea level rise and sea surface temperature. Sea level rise is now taken into account when designing coastal constructions and should be taken into account when developing the infrastructure of coastal cities, along with regional adaptation strategies for future climate change consequences. Additionally, it highlights that all design storm events must be considered as wind and wave patterns occur at the corresponding high water levels (HWL; defined as storm surge), which is the sum of the astronomical tide and seasonal variation amplitudes.

In a study conducted by Besiktepe et al. (2011) in Izmir Bay, a model that can predict the current, temperature and salinity of Izmir Bay based on real data was developed and the forces activating the Gulf currents were examined. The circulation of the Izmir Bay was investigated using data-based simulations from the Harvard Ocean Prediction System and a simple equation model. The components of the sub-basin scale circulation were determined using simulations. The size, structure and evolution of the primary circulation are consistent with the observations. In this study, it was concluded that the main circulation of the bay is a cyclonic eddy that covers almost the entire basin. Wind and offshore forcing are responsible for driving and modifying this circulation. Also, due to the characteristics of the coastline, currents in the Inner Bay are generally quite weak and water exchange between the Inner Bay and the Middle Bay is limited. As a result, the inner gulf develops a cyclonic cycle the size of a basin. Since the channel is

very small and has a maximum depth of about 10 meters, there is a threshold between the inner and middle gulfs. This barrier limits the amount of water that can enter the bay. On the other hand, due to the shallowness of this region, the currents coming from the north from the inner gulf are weakened by ground friction and become another factor that restricts water exchange. In addition to the threshold at the mouth of the inner gulf and the shallows in the north, the loops formed in the middle gulf also play an inhibitory role in the water exchange between the inner bay and the outer bay.

Kisacik et al.(2016) have a project study to protect İzmir from coastal floods. The aim of these project is to reduce wave flooding throughout the Kordon region by experimentally examining the use of a new coastal protection structure profile known as the Stilling Wave Basin (SWB). The seaward vertical wall consists of two rows of walls, the gently sloping pool and a second crown wall towards the land from the SWB. The sea-facing wall causes the waves to be driven upward before they "die and fall" and lose energy in the sloping basin. Because the sea-facing wall is essentially a double row of moving barriers, excess water can be drained away. When there is a significant overflow, the water loses energy as it flows back and forth in the basin between the crown walls toward the sea and towards the land. The land-facing crown wall cannot be overcome by the available energy. The barrier coefficient, the ratio between the open and closed portions of both rows of slid walls, is a very important SWB metric. Therefore, the best balance between entry (as low as possible) and exit (as high as possible) must be explored to avoid increasing the crest freeboard.

CHAPTER 3

DATA USED

In this study various kind of wind, sea water level and bathymetry data were used to investigate the coastal flood in Izmir Bay. In this section details of data used during the study are explained.

3.1. Wind Data

Wind is the main source that generates the wave and it may also cause a rise in the water level. For this reason, it is very important to determine the features such as wind speed and direction correctly and the annual and extreme characteristics of the wind. Wind data can be obtained from in-situ measurements or numerical model results. In this study, two wind data sets were used 1) in-situ measurement data carried by Izmir Metropolitan Municipality and 2) the ERA5 dataset, which is the newest re-analysis model result provided by the European Medium Range Weather Forecasts Center.

3.1.1. In-situ Measurement Data

There are in-situ wind measurement stations of Izmir Municipality to be used for various purposes. For this study, the wind data were obtained from three stations. These stations are;

-Foca

-Pasaport

-Bostanli

Pasaport and Bostanli stations are placed at inner bay. The data at these three stations have been available since 2017 making almost 5-year data set. Not only wind speed, and direction, but also air pressure, precipitation, water level and water temperature are measured at these stations. An example station data set is shown in Figure 3.1. Wind speed and wind direction data are recorded for 10-minute period with 1 s intervals. The maximum, average and std deviation values of 10 mins record are given as can be seen in Figure 3.1. The measuring device in the station continue to record data in

case of malfunction or during routine maintenance. Therefore, there may be incorrect measurement data in the data set. The error may be due to the device or external factors. Some erroneous data is shown in Figure 3.2. In this study, attention was paid and erroneous data were removed firstly.

	Wind Spd (Avg.) (m/s)	Wind Spd (Max.) (m/s)	Wind Spd (Sde.) (m/s)	Wind Dir. (Avg.) (Â°)	Wind Dir. (Max.) (Â°)	Wind Dir. (Sde.) (Â°)	Atm.Press (Avg.) (mb)	Rain (Accu.) (mm)	Rain (Max.) (mm)	Water L.1 (Avg.) (cm)	Water L.1 (Max.) (cm)	Water L.1 (Min.) (cm)	Water Temp (Avg.) (Â°)
Time	Full Time	Full Time	Full Time	Full Time	Full Time	Full Time	Full Time	Full Time	Full Time	Full Time	Full Time	Full Time	Full Time
Med.	3.919	--	0.801	178.664	--	--	--	0.011	--	--	--	--	--
MÃ¡x.	--	97.702	--	--	--	--	--	13.8	--	--	--	--	--
	(--)	(16:30)	(--)	(--)	(--)	(--)	(--)	(04:10)	(--)	(--)	(--)	(--)	(--)
MÃ-n.	--	--	--	--	0.113	--	--	0	--	--	--	--	--
	(--)	(--)	(--)	(--)	(09:40)	(--)	(--)	(00:00)	(--)	(--)	(--)	(--)	(--)
Acu.	--	--	--	--	--	--	--	546.602	--	--	--	--	--
1.1.2017 00:00	2.754533	4.842875	0.669997	107.3605	111.4472	10.82458	1023.895	0	0	22.15563	22.15709	22.15314	12.122
1.1.2017 00:10	2.829592	4.085126	0.437357	100.6958	87.27879	7.841707	1023.894	0	0	22.1562	22.15731	22.15464	12.074
1.1.2017 00:20	2.402008	4.133661	0.508309	103.777	104.4997	11.74706	1023.895	0	0	22.15649	22.15796	22.15487	12.01
1.1.2017 00:30	1.658015	3.743277	0.622633	117.4688	96.85818	22.94252	1023.895	0	0	22.15723	22.15873	22.15569	11.961
1.1.2017 00:40	1.154699	2.326767	0.284191	178.9305	156.762	22.3339	1023.858	0	0	22.15807	22.15914	22.15652	11.951
1.1.2017 00:50	1.370546	2.716192	0.363539	213.4306	202.0969	9.334249	1023.747	0	0	22.15904	22.16011	22.15716	11.967
1.1.2017 01:00	1.540056	3.276926	0.599248	213.6159	205.6038	26.01719	1023.744	0	0	22.16015	22.16136	22.15849	11.973
1.1.2017 01:10	1.411332	3.695126	0.70874	171.14	277.9869	58.55079	1023.746	0	0	22.16067	22.16176	22.15875	12.034
1.1.2017 01:20	3.496885	6.159055	1.193058	101.4395	62.15938	17.04961	1023.67	0	0	22.16098	22.16227	22.15891	12.001

Figure 3.1. Example of in-situ measurement station dataset

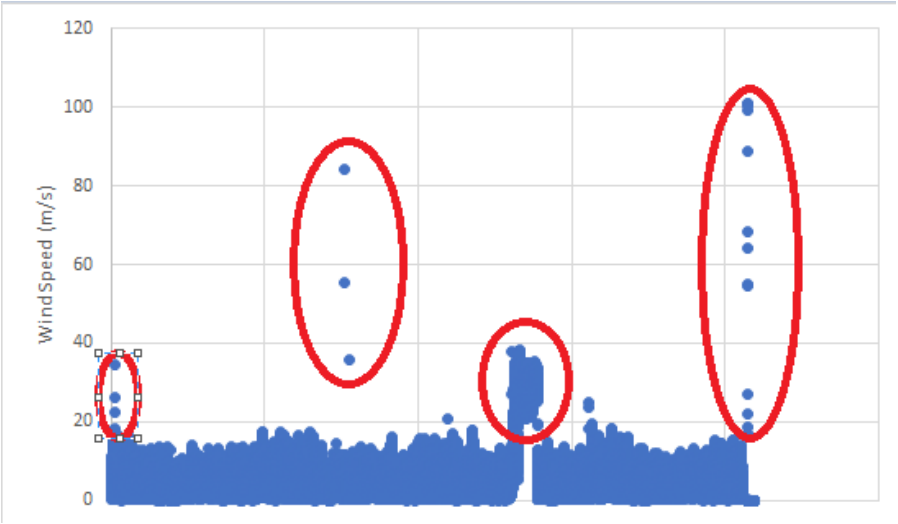

Figure 3.2. Some erroneous wind speed data (in red circle)

3.1.2. ERA5 Dataset

For this study, a long dataset is necessary to determine the wind climate and extreme value analysis. Izmir Municipality's in-situ measurement data are not suitable since it is just a 5-year data set. Therefore, a long dataset was looked for. There are meteorological agencies around the world that produce models for wind estimates at the past. One of the global suppliers of long-term reanalysis wind data is the European Center for Medium-

Range Weather Forecasts (ECMWF). ECMWF's newest reanalysis dataset is ERA5 and is being developed as a part of the Copernicus Climate Change Service (C3S) (Ozbahceci et al, 2020). The ERA5 provides hourly estimates of wind dataset covering the period from 1979 to the present. The wind data on the sea surface are available on a 40-km grid distance (Hersbach et al., 2020).

For this study, 42 years of ERA5 wind data were downloaded from the website https://cds.climate.copernicus.eu/cdsapp#!/dataset/reanalysis-era5-single-levels?tab=form. Data downloading steps are shown in Figure 3.3. The ERA5 dataset can be downloaded as a GRIB file. A software program called Panoply was used to convert the grib file to a text file. A MATLAB code was written to select the data in the desired coordinate. The point chosen for the wind data is at the coordinates of 38.8N – 26.5E at a point close to the entrance of İzmir Bay. This point is seen in Figure 3.3.

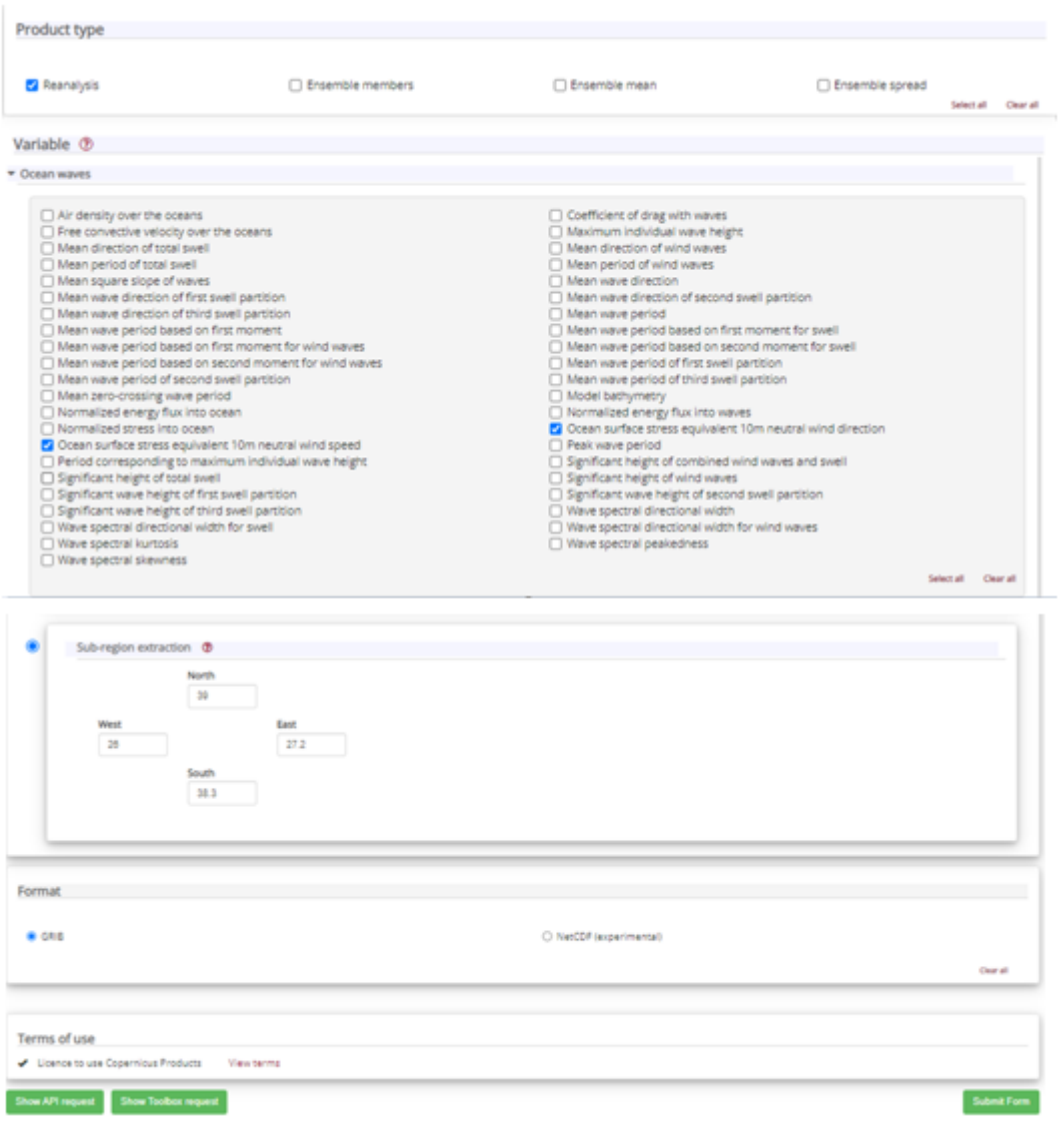

Figure 3.3. Web interface where Era5 data sets are downloaded

3.2. Sea Level Data

In this study, 3 data sets were used to determine the fluctuations in sea water level changes. Two of these are in-situ measurements of water level data obtained from the Bostanli and Pasaport which are the measurement stations of the Izmir Municipality, and the other is the data obtained from Mentes mareograph station of the Turkish National Sea Level Monitoring System (TUDES).

3.2.1. Izmir Municipality Sea Level Measurement Stations

The sea level data obtained from Bostanli and Pasaport stations of İzmir Municipality are between 2017 and 2021 The water level measuring devices in those stations are acoustic-type measurement devices. Data are recorded at 10-minute intervals. The average, the maximum and the minimum values over the 10-minute period are provided. In-situ data are calibrated according to Turkish vertical reference frames (TUDKA-99). When the water level data were analyzed, it was seen that there are also incorrect values in the data set. These erroneous data were removed from the data set with the help of using MS Excel and a Matlab code written by the author. The sea level measurement station of Izmir Municipality in Bostanli is shown in Figure 3.4.

Figure 3.4. Bostanli sea level measurement station

3.2.2. TUDES Mareograph Station

In our country with long coasts, mareograph stations are operated by the Turkish Sea Level Monitoring System (TUDES) of General Directorate of Mapping in order to provide current and future sea levels which may be necessary for the construction and city planning works and to monitor long-term sea level changes on our coasts. The map of TUDES mareograph stations is given in Figure 3.5.

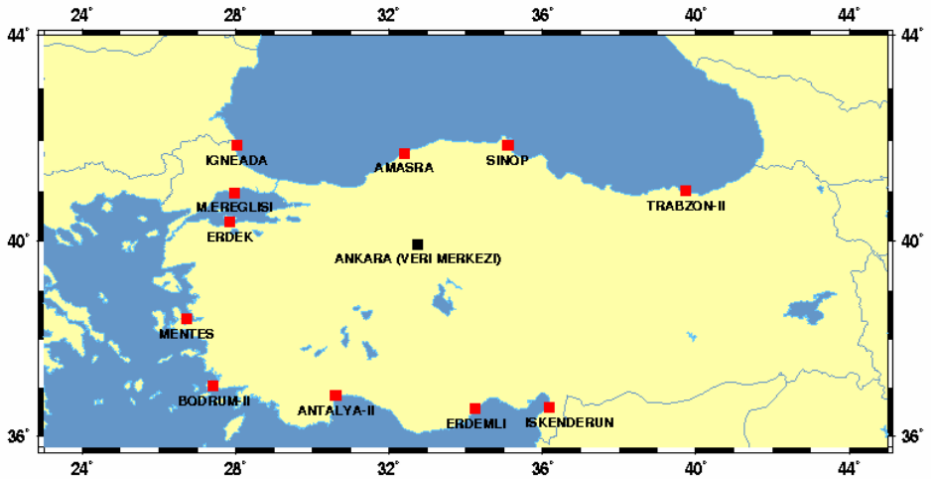

Figure 3.5. Turkish National Sea Level Monitoring System (TUDES) (www.hgk.mil.tr)

In this study, TUDES mareograph station data in İzmir Mentes was used. TUDES Mentes Station data is a 21-year (2000-2020) data set and the measuring device in the station is acoustic type. Average sea level data were provided with 10-minute intervals in 2000 and 2001, and 15 minutes intervals in the rest of the years. This dataset only has a 2-month (April-May) interruption in 2009. Contrary to in-situ sea level measurement data, the free version of TUDES data are not calibrated according to Turkish vertical reference frames (TUDKA-99). The TUDES mareograph station is shown in Figure 3.6.

Figure 3.6. TUDES mareograph station

3.3. Bathymetry Data

The precision of a wave model's estimate result is directly correlated to the availability of correct and high-resolution bathymetry data. The resolution of the bathymetry data should be as high as possible for the most accurate results to be obtained from the model. In this study, bathymetry data provided by the Izmir Municipality and Dr Gökhan Kaboğlu from the Marine Science and Technology Institute of 9 Eylul University are used. The bathymetry data are obtained as X, Y, and Z data and converted to the regular grid bathymetry data with a 5m interval using Blue Kenue software developed by National Research Council Canada and introduced to numerical wave model SWAN. Figure 3.7 illustrates the bathymetry of Izmir Bay after converting to the regular grid.

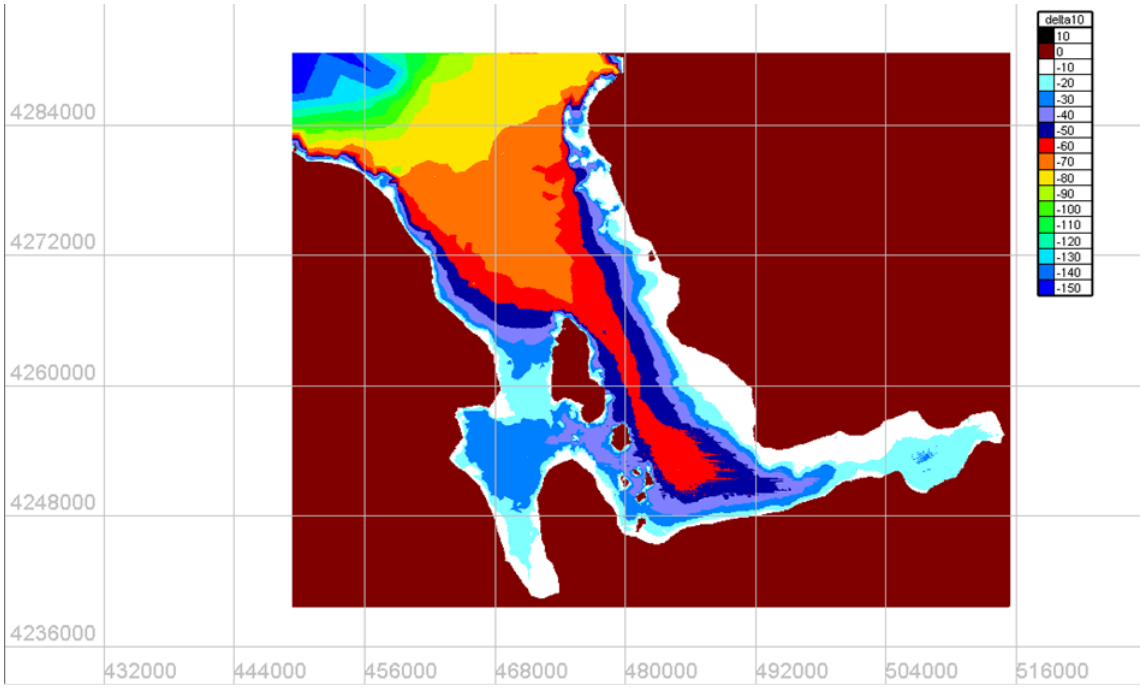

Figure 3.7. Izmir Bay Bathymetry Map (The brown part is land)

As can be seen in Figure 3.7, the research area that encompasses the whole of Izmir Bay is shaped as a rectangle with dimensions of 65 kilometers horizontally and 55 kilometers vertically. The max water depth in the inner Bay is 60m.

CHAPTER 4

WIND CLIMATE

Long-term wind analysis to determine the characteristic of the winds are called as wind climate analysis. Wind climate analysis has two purposes: 1) To organize the wind data and to extrapolate the data to extreme values with low probability of occurrence (Kamphius, 2020). This section explains the details of wind climate analysis performed in this study.

4.1. Compatibility of ERA5 and In-Situ Measurement Data

Although ERA5 is one of the most consistent and high-resolution open datasets for climate computations (Ozbahceci, 2019, Ozbahceci et al.,2020), it must be validated before being utilized in wind climate studies. The data from the Izmir Municipality's in-situ measuring station in Foca was found suitable for the verification analysis in this study. Because the Foca station is the closest one to the location where ERA5 data is collected. Figure 4.1. indicates the locations of Foca station and the ERA5 data point.

Figure 4.1. ERA5 data and Foca wind measurement locations

It is known that the measurement station at Foca is at an altitude of 15 meters above sea level. However, ERA5 data provides the wind speed at 10 m above sea level

(u_{10}). Therefore, Foca wind speed values were converted to u_{10}, firstly using the following equation (Kamphius, 2020).

$$\frac{U_{10}}{U_z} = \left(\frac{10}{z}\right)^{\frac{1}{7}} \qquad (1)$$

Then wind speed data of ERA 5 and Foca stations were compared as a time series in Figure 4.2. Good agreement was observed between Foca data and ERA5 data. As seen in Figure 4.2, the high and low wind speed values of Foca and ERA5 data seem match generally.

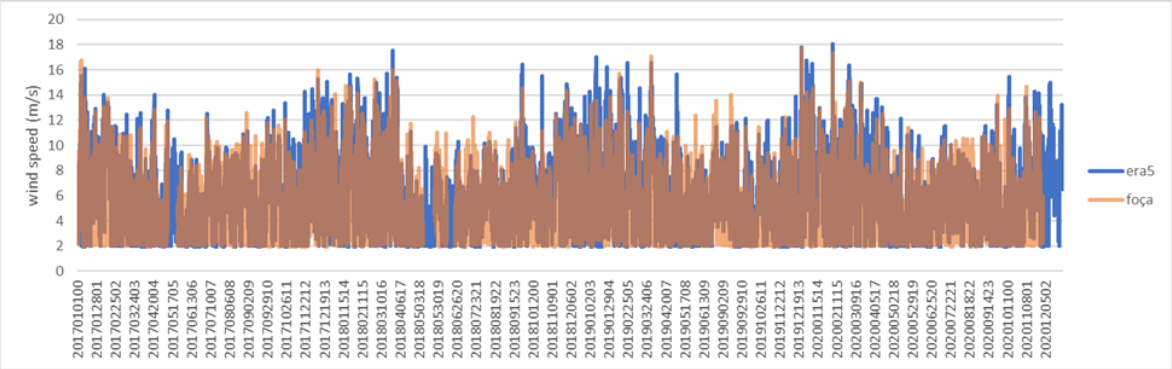

Figure 4.2. ERA5 and Foca wind speed time series comparison

However, when a, a scatter graph was plotted using data of Foca and Era5 as shown in Figure 4.3, two wind speed datasets are correlated but highly scattered.

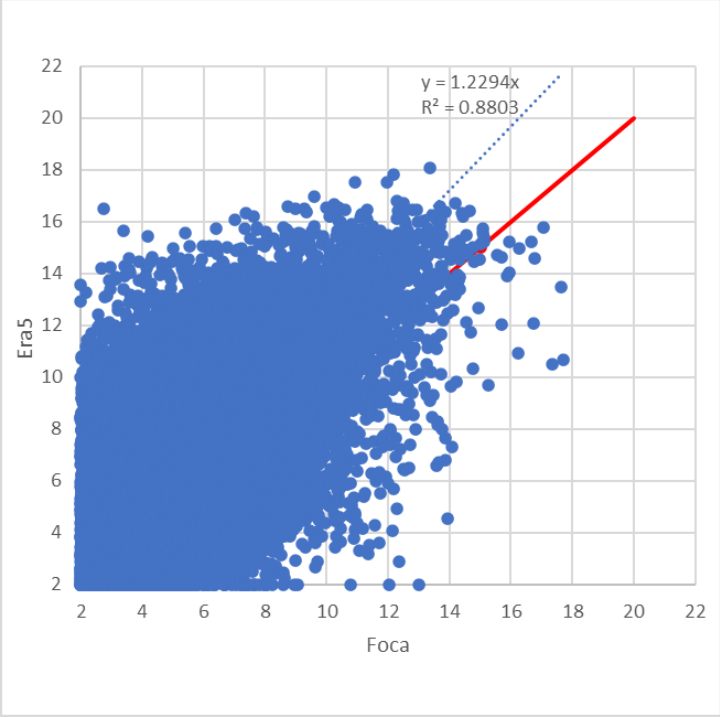

Figure 4.3. Scatter plot of ERA5 and Foca station wind speeds

In addition, statistical error measures of Root Mean Square Error (RMSE), BIAS, Mean Absolute Error (MAE) and Scatter Index (SI) were calculated and given in Table 4.1. Definitions of the error measures are given below:

$$RMSE = \left[\frac{1}{N}\sum_{i=1}^{N}(P_i - O_i)^2\right]^{\frac{1}{2}} \quad (2)$$

where; P_i is ERA5 data O_i is Foca data

$$SI = \frac{RMSE}{\bar{O}} \quad (3)$$

The model performs better when the RMSE and SI parameters are near to zero. $\bar{O_i}$ in the Eq. (3) represents the average of the Foca values.

The disparity between ERA5 data and the average of Foca data is referred to as bias. When the bias is zero, the condition is known as objectivity.

$$BIAS = \bar{P_i} - \bar{O_i} \quad (4)$$

Mean Absolute Error, it is the average of the absolute differences between Era5 and Foca. Formula,

$$MAE = \sum_{i=1}^{N}\frac{1}{N}(|P_i - O_i|) \quad (5)$$

Table 4.1. Error values for wind speed of Era5 and FOCA data

RMSE(m/s)	Bias(m/s)	Mae(m/s)	SI
2.85	1.12	2.24	0.56

When the data is analyzed for a shorter time period, it is seen that there is a time difference between ERA5 and Foca data, as seen in Figure 4.4. This time difference may be an expected result because of the distance between the two locations. In Figure 4.4, it was noticed that the peaks almost coincided when the ERA5 data was shifted 3 hours. This time difference varies between 2 and 4 hours for other high-speed wind cases.

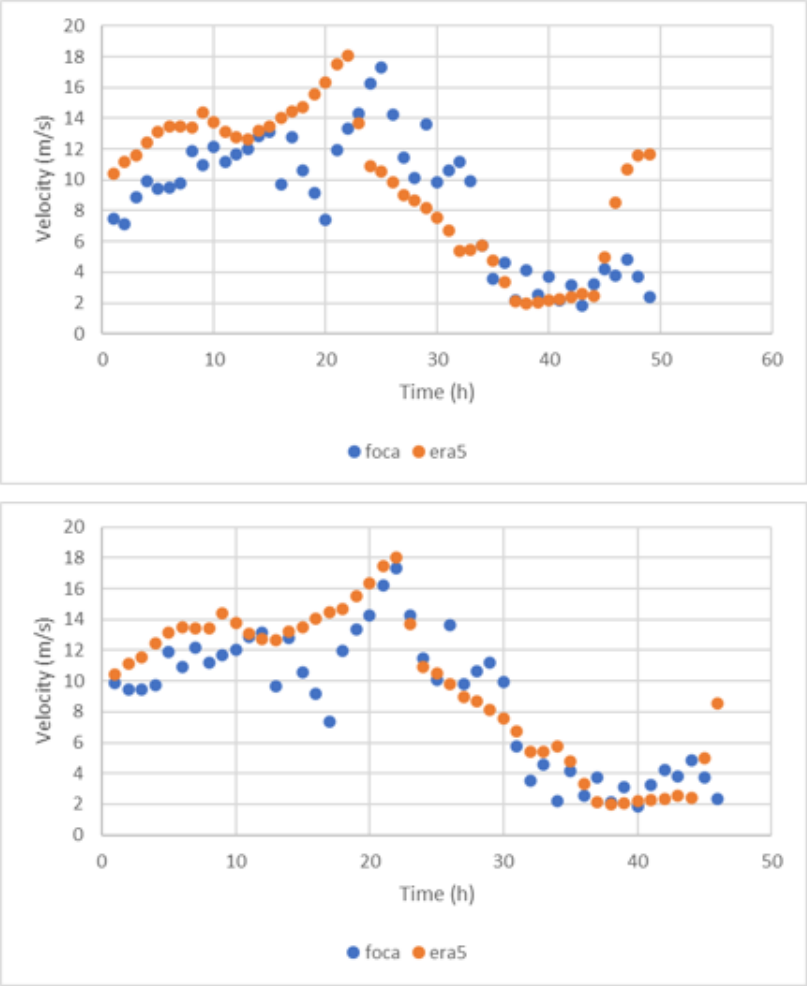

Figure 4.4. Time-series comparison with existing time gap (top) and after shifting (bottom)

After ERA5 wind speed data are shifted 3 hrs, the error measures were calculated again and the results are given in Table 4.2.

Table 4.2. Error values for wind speed of Era5 and Foca data after 3hrs shifting

RMSE (m/s)	Bias (m/s)	Mae (m/s)	SI
2.740329	1.115919	2.150338	0.538605

As can be seen in Table 4.2 there is a slight decrease in error measures after shifting the ERA5 data 3 hours.

Since the higher winds are more critical for the coastal flood point of view, the maximum daily wind speed data of Foca and ERA5 are compared in Figure 4.5, and the re-calculated error measures are given in Table 4.3. Figure 4.5 shows that the maximum

daily wind speeds of ERA5 and Foca are highly correlated and less scattered compared to whole data comparison given in Figure 4.3.

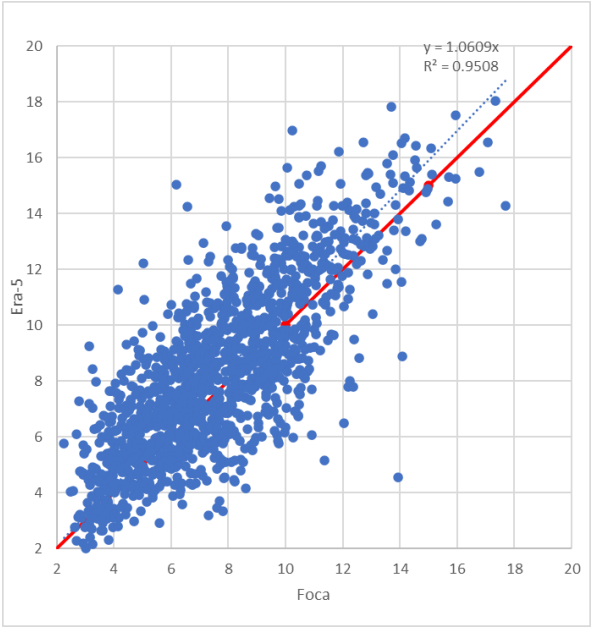

Figure 4.5. Comparison of the maximum daily wind speeds between ERA5 and Foça

Table 4.3. Error measures for maximum daily wind speed of Era5 and FOCA data

RMSE	Bias	Mae	SI
2.02	0.60	1.58	0.26

As can be seen in Table 4.3, error measures are much lower than the error results of whole data given in Table 4.1 and 4.2.

In Figure 4.6, the U_{10} values of Foca and ERA5 are plotted. Wind speeds higher than 10 m/s are used in this graph.

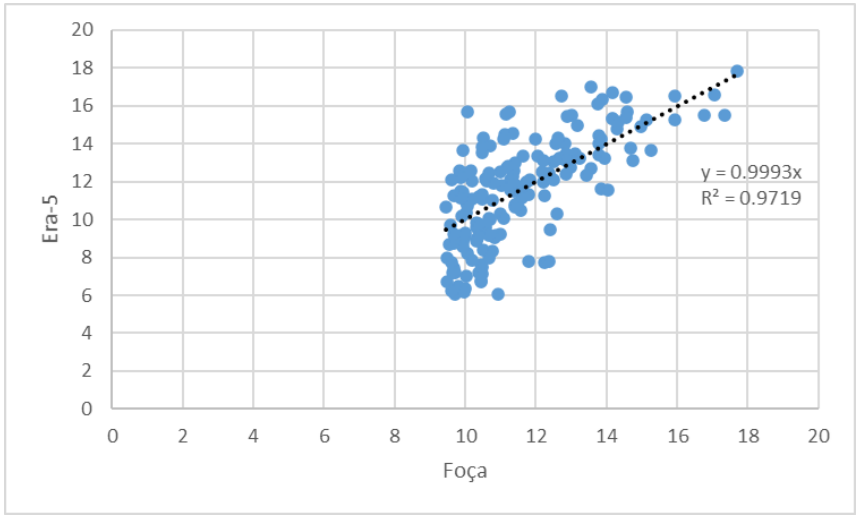

Figure 4.6. Comparison of Era5 and Foca station according to U_{10}

Figure 4.6 also shows that there is a good agreement between the ERA5 and Foca wind speed data for the higher wind speeds which are more critical for the coastal flood study.

4.2. Wind Rose

The wind rose is a graphical tool that shows how wind speed and direction are typically distributed at a specific region. In Figure 4.7, the wind rose of Foca station is shown. The prevailing wind directions for Foca seem to be North East (NE) and North North East (NNE).

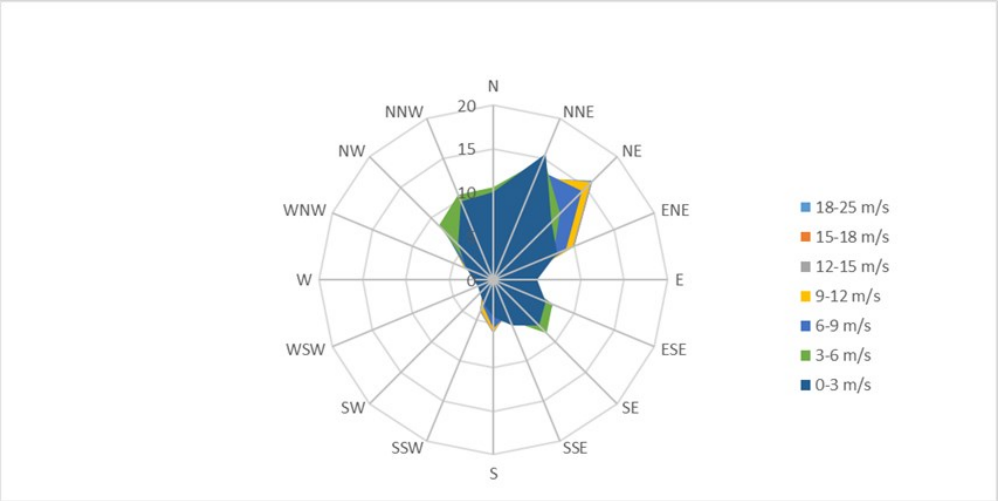

Figure 4.7. Foca in-situ measurement station wind rose

In Figure 4.8, the wind rose with the 5-year (2017-2020) data of the ERA5 data is seen. The prevailing wind direction of the ERA5 data is North North East (NNE).

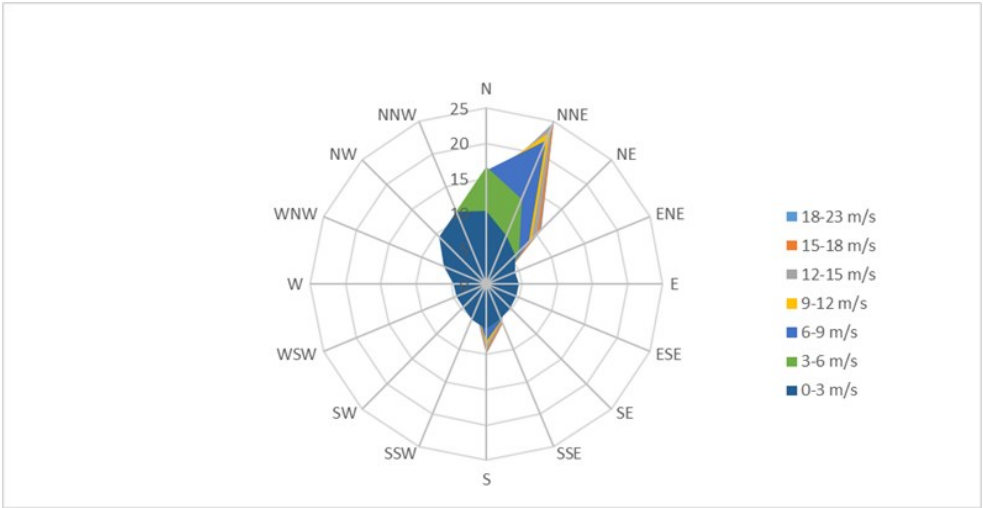

Figure 4.8. Era5 wind rose (2017-2020)

As a result of these comparison studies, it is seen that there is a good agreement between the higher wind data of the Foca in-situ measurement station and the reanalysis model ERA5. Therefore, it is concluded that ERA5 data can be used in wind climate study. Accordingly, the wind rose created by ERA5's 42-year hourly data is shown in Figure 4.9. The prevailing wind direction is again North North East (NNE). In addition, South and South East winds are found to be effective.

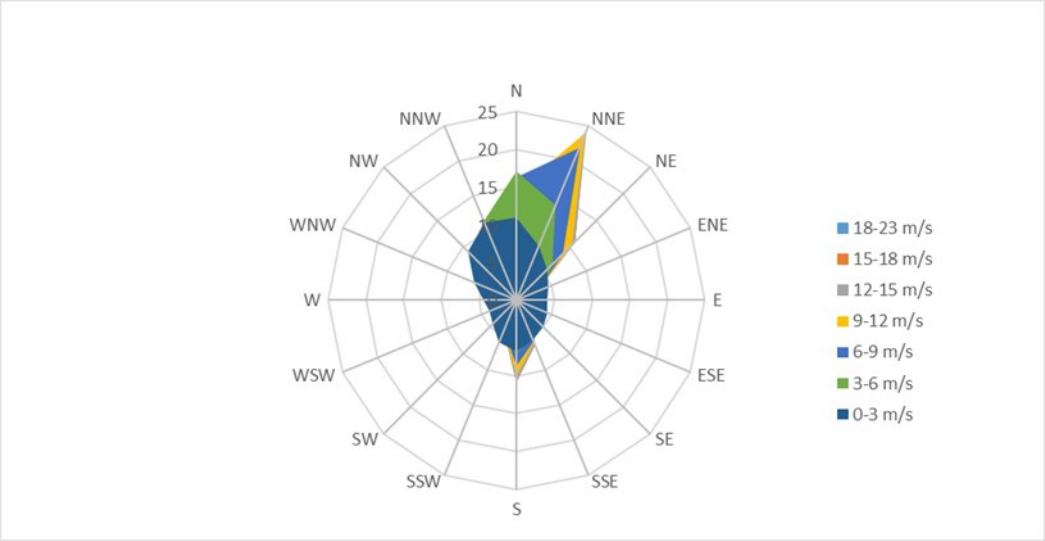

Figure 4.9. Era5 wind rose

4.3. Extreme Value Statistics for Wind Speed

The purpose of extreme value calculation is to estimate the expected value of an extreme event that will occur once in a long period. This long period is called the return period (Rp). In extreme value analysis, firstly, the cumulative distribution of the data is made and a distribution function is created. Extrapolating the data set to extreme values corresponding to longer return times with lower probability requires fitting to a distribution function (Kamphius, 2020). After that, because the parent distribution is usually unknown, the best-fitting distribution is analyzed.

For the analysis of extreme values, maximum annual data or data selected by the POT method are used by sorting. In this study, maximum annual wind speed data for 42 years was used. First, the probability of not exceeding the wind speeds listed in descending order is calculated. The best-known formula for calculating the probability of not being exceeded is the corrected Weibull formula given in Eq.(6) (Goda, 2010).

$$P(x) = (m - \alpha)/(N + \beta) \quad (6)$$

where; P(x) = probability of non-exceedance, m= order number, N=data number, a and b are coefficients changing according to the used theoretical distribution function.

The below are the cumulative distribution functions of the most commonly used distributions (Goda, 2010).

Fisher Tippet I (Gumbel)

$$P(x) = exp[-exp\,(-(x - B)/A)] \quad : -\infty < x < \infty \quad (7)$$

Fisher Tippet II

$$P(x) = exp[-(1 + (x - B)/kA)\text{^}(-k)\,] \quad : B - kA < x < \infty \quad (8)$$

Weibull

$$P(x) = 1 - exp[-((x - B)/A)\text{^}k\,] \quad : B \ll x < \infty \quad (9)$$

Log-normal

$$P(x) = \int p(t)dt \quad : 0 < x < \infty$$

$$p(x) = 1/(\sqrt{2\pi}\,Ax)\; exp[-(lnx - B)2/(2A2\,))] \quad (10)$$

where; A, B, and k are scale, location, and shape parameters, respectively.

The A, B, and k parameters are obtained by fitting a distribution function to the calculated non-exceedance probabilities of the wind data. The least-squares approach, the method of moments, and the maximum likelihood method are ways of obtaining these parameters. The least-squares method was used in this study. Gumbel, Log-normal, FisherTippet II (k = 2.5, 3.33, 5.0, and 10.0) and Weibull (k = 0.75, 1.0, 1.4, and 2.0) distributions were employed as candidate distributions to investigate the best distribution function. Then, the compatibility is tested using the square of the correlation coefficient, the MIR Criterion (Minimum residual ratio cor. coff.), the DOL criterion (OutLier Deviation), and the REC criterion. Details of these tests can be found in Goda (2010).

After determining the optimal distribution, the extreme value corresponding to any return period (in years) is calculated using Equation (2.6) with the inverse function of the cumulative distribution:

$$xRp = F - 1\,(1 - 1/\lambda Rp) \quad (11)$$

where; λ is the annual average rate or number of sample data. When the annual maximum wind speed is used, λ=1.

As a result of the extreme wind speed analysis, the best fit was found in the Gumbel distribution. In Figure 3.18, the data fitted to the Gumbel distribution for the

North direction is shown with 95% confidence interval curves. From Figure 4.10, it is possible to read the wind speeds corresponding to 50, 100, 200, and 500 year return periods on the upper x-axis from the data on the y-axis. Accordingly, the speed of the wind blowing from the north for Rp= 100 years is approximately equal to 20.3±2.0 m/s.

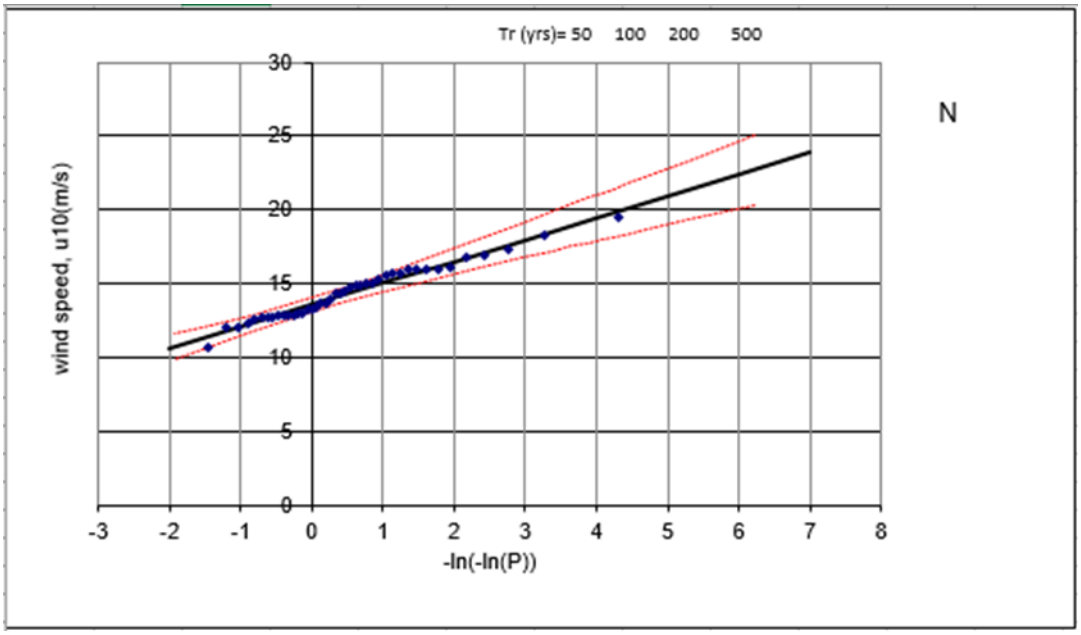

Figure 4.10. Extreme wind speed analysis by Gumbel distribution for the North direction

Wind speeds with a 100-year return period were calculated for each direction that can generate the waves using the extreme wind speed analysis and results are given in Table 4.4.

Table 4.4. Wind speeds with 100 years return period

	Wind speed (m/s)		
	Upper Limit	TR=100 years	Lower Limit
N	22.08	20.33	18.58
NNW	18.60	17.09	15.58
NW	18.60	16.93	15.26
WNW	19.44	17.64	15.84
W	20.28	18.31	16.34
WSW	20.13	18.33	16.53
SW	20.22	18.61	16.99
SSW	20.25	19.01	17.77
S	21.63	20.52	19.41
SSE	22.62	21.17	19.72
SE	19.54	17.96	16.39

CHAPTER 5

FLUCTUATIONS IN SEA WATER LEVEL

One of the important parameters in the design of coastal structures is the sea water level. There are many parameters that affect the sea water level. Due to these parameters, the sea water level changes even during the day. Where the waves break and loose most of their energy depends on the water level. For this reason, the exposure of structures to high waves is related to the sea water level. As the water depth increases, the wave breaks closer to the shore and can damage the structure and the areas behind it. Therefore, most damage occurs when water levels are high (Kamphius,2020). Sea water level changes are classified as follows according to the recurrence period and frequency of occurrence;

— Short Term: Tides, Storm Surge, Barometric Surge and Wave Setup

—Seasonal

—Long Term: Sea Level Rise Due to Climate Change

—Rare and Extreme incident: Hurricanes and Tsunamis

Short-term and seasonal fluctuations are taken into account in the design of coastal structures. Short-term and seasonal fluctuations have statistical characteristics. Long-term water level changes are not traditionally considered but are known to be necessary for the design. Rare and extreme level changes are normally ignored as they increase the cost of construction and occur at very long and irregular intervals.

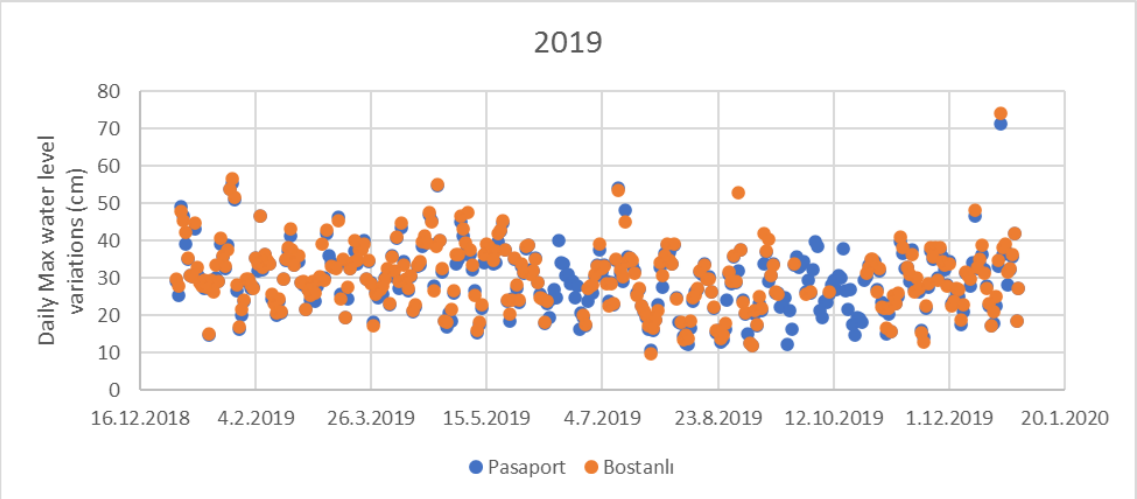

Figure 5.1. Calculated maximum daily variations in sea level for Bostanli and Pasaport measurement points in 2019

In this study seawater level data measured at Bostanlı and Pasaport stations and measured at Mentes Mareograph station are used. The details of the data used are given in Chapter 3. Figure 5.1 shows that there is a very good agreement between the Pasaport and Bostanli measurement sea water level data. They are also compared by a scattered plot, provided in Figure 5.2. As can be seen in Figure 5.2, correlation is very good between Bostanli and Pasaport data. Good correlation is also a verification of the measurements.

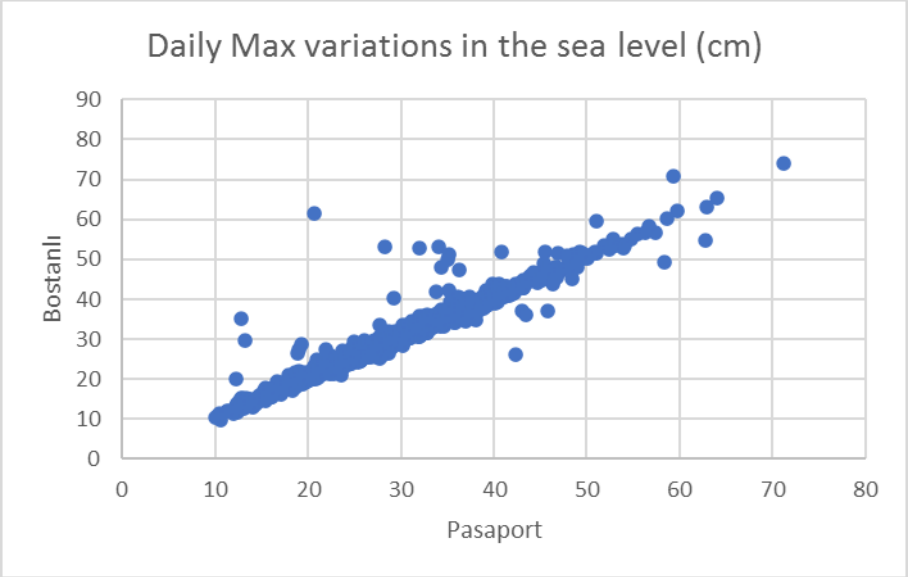

Figure 5.2. The comparison between Pasaport and Bostanli data

5.1. Storm Surge

During the storm, water level may increase due to wind set-up and wave set-up.

5.1.1. Wind set-up

Wind set-up is a temporary increase caused by the shear force of the wind on the water surface. Because the same wind can create large waves, the combination of high waves and high-water level can cause coastal damage and flooding (Collins et al., 2019).Seawater is pulled by the wind when a strong wind blows in a shallow bay for an extended period. Seawater builds up in the coastal zone when the wind is onshore, raising

the sea level. The following equation gives the sea level increase η0 (cm) at the coastline if the angle (α) between the wind direction and the line perpendicular to the beach:

$$\eta_0 = k\frac{F}{h}(U * cos\alpha)^2 \quad (12)$$

where, F is fetch length (km), U is wind speed, h is mean sea depth, and k is constant. The k value changes according to the characteristics of the bay. In studies conducted in the Baltic Sea, k= $4.8*10^{-2}$ was found (OCDI,2009).

For storm surge analysis, data on high wind days were analyzed, and for this, we worked with wind and water level data in Pasaport and Bostanli.

Figure 5.3 shows the change in wind speed and water level during a storm that occurred in Bostanli on 16.01.2018. As seen in this example, there can be a high rise in water level at high wind speeds.

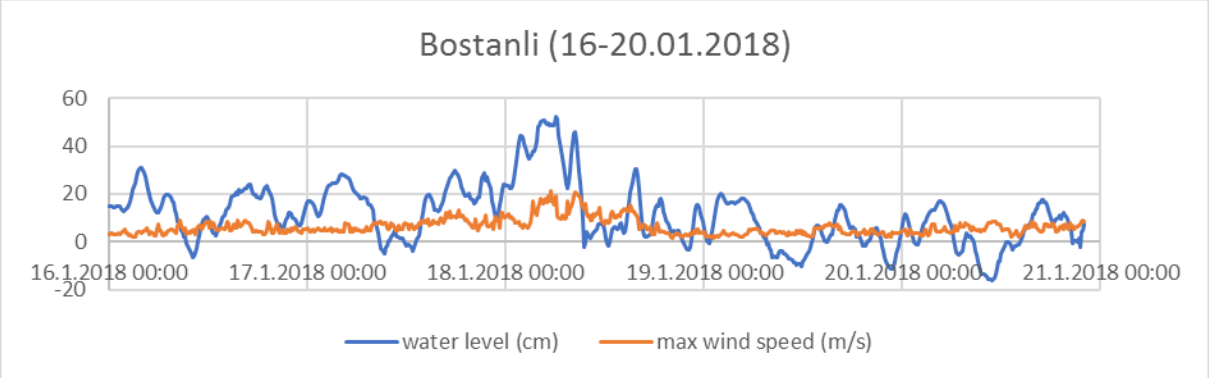

Figure 5.3. Change of wind speed and water level during a storm in Bostanli

Using the data of the day (16-20 January 2018) in Equation 12 and Figure 5.3, the amount of increase in the water level due to the wind setup was calculated as 17 cm. In this calculation, F=6 km, h=2 m, U= 11 m/s and α=0 are accepted.

5.1.2. Wave Setup

The rise in mean water level that occurs along the coast when small waves break is known as wave setup. Wave setup, a factor in storm-induced damage and coastal flooding, is critical since it is one of the factors that make up storm surges (Guérin et al., 2018).The amount of sea level rise resulting from the wave setup can be found in Figure 5.4. This chart was created with the random wave breaking model. Here are the parameters affecting the sea level change; The slope of the seafloor, related to wave height

and wavelength (Goda,2000). According to this graph, a sea level rise of 13 cm is calculated with wave height of 1 meter, wave period of 4 s, and seafloor slope of 1/20.

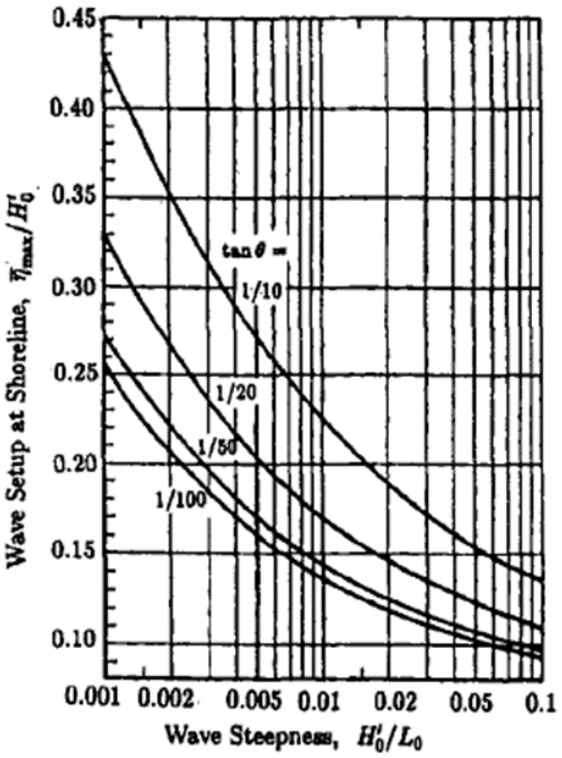

Figure 5.4. Wave setup calculation chart

When the 5-year is examined in the Bostanli data, the time when the average water level was maximum was realized on 23.12.2019. As seen in Figure 5.5, while the average water level was around 20 cm before the storm, it increased to 75 cm with the storm due to storm surge.

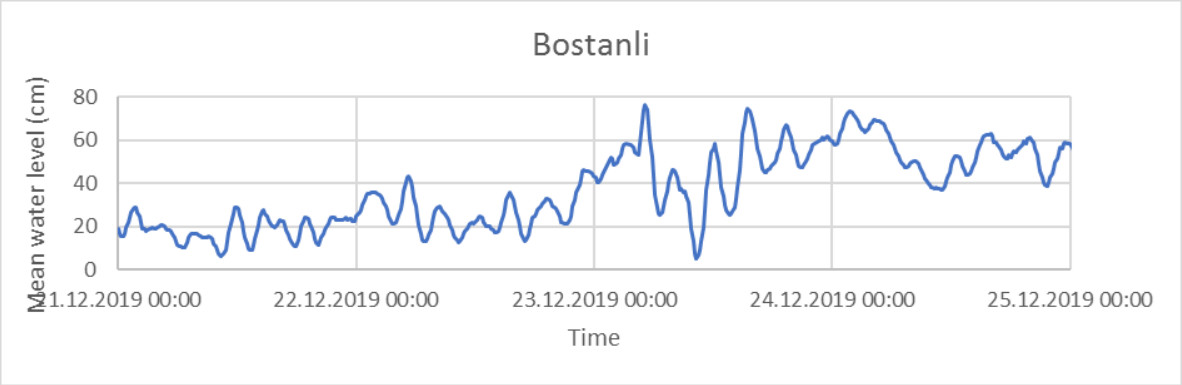

Figure 5.5. The maximum increase in the mean water level in 5 years data

5.2. Barometric Surge

Another effect on sea water level changes is barometric effects. Air pressure can change with strong winds. With the wind, the air pressure decreases. If the atmospheric pressure decreases, the sea level rises. This interaction of sea level is called the reverse barometer effect. The level of the sea surface varies in accordance with the following equation, depending on the mean sea level.

$$\Delta h = \frac{\Delta P}{\rho g} \tag{13}$$

where, Δh is sea water level change, ΔP is atmospheric pressure change, p is seawater density, g is gravity mass.

Considering g=9.81 m/s2 and if ρ=1026 kg/m2 for sea water,

$$\Delta h = 0{,}993\ \Delta Pa \tag{14}$$

Therefore, 1 millibar change in atmospheric pressure causes 1 cm change in sea level (Pugh, 2004).

The pressure on the sea surface is also measured at the Bostanli and Pasport stations. The relationship between sea level and pressure was examined with these two data sets. As seen in the scatterplot in Figure 5.6, although there is scattering, it can be said that there is a tendency to increase in water level when the pressure decreases.

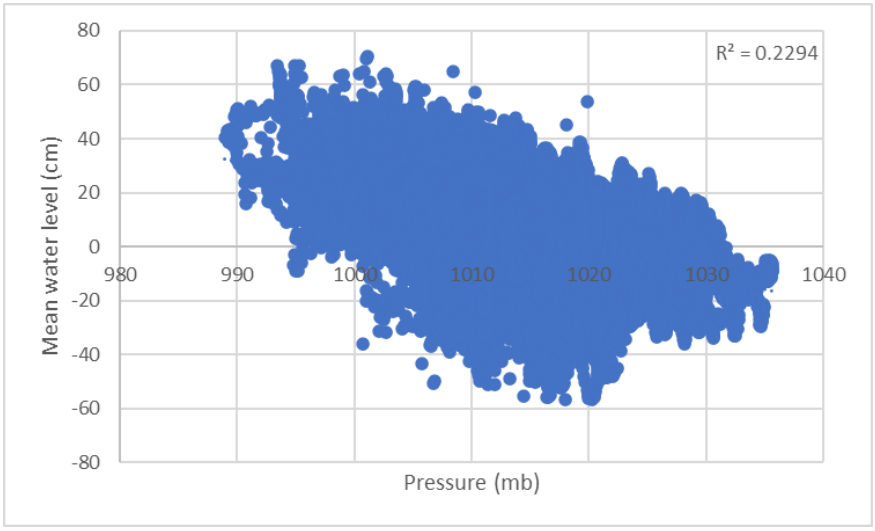

Figure 5.6. The relation between the pressure and sea water level

In Figure 5.7, wind, pressure and sea water level are examined together. For this, a day with high wind speed was chosen. In these data of 25.01.2019, the average wind

speed increased from 4m/s to 17m/s, while the sea water level increased from 20cm to 70cm. Meanwhile, with the increase in wind speed, the atmospheric pressure decreases from 1007mb to 997mb. Moreover, the sea level increases due to barometric reasons and storm surge.

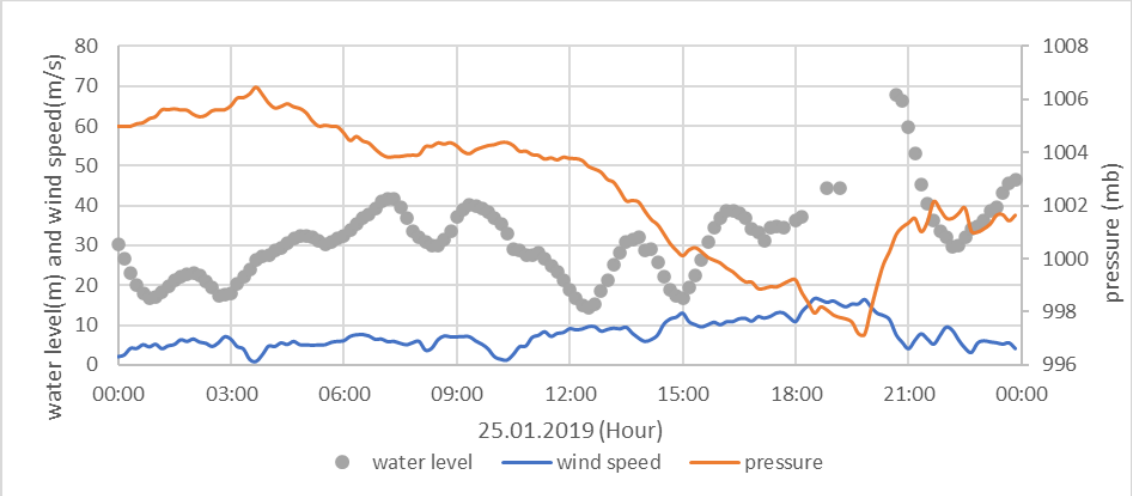

Figure 5.7. Sea water level, atmospheric pressure and wind speed on 25.01.2019

When the sea level is examined in Figure 5.7, there is a 50 cm increase in the water level. There has been a decrease of approximately 10 mb in the atmospheric pressure. According to Eq. (14) given above, almost10 cm of the 50 cm increase in the sea water level was caused by barometric reasons.

5.3. Tides

Astronomical tides play a decisive role in sea level fluctuations in coastal areas. They cause the rise and fall of the water level and can sometimes cause currents at great speeds. Tides directly affect coastal morphology, navigation, fishing and habitat. Tides are the result of a combination of forces acting on water particles. These forces (Kamphius, 2020):

— the earth's gravitational attraction,

— the centrifugal force caused by the rotation of the earth-moon pair,

— the moon's gravitational attraction,

— the sun's gravitational attraction.

The tides cause not only sea level changes but also vertical changes in large lakes, the atmosphere and the solid earth crust, but these changes are much lower than the changes in sea level (NOAA 1998).

In this study, to calculate the daily tide firstly, the mean water level was checked in the absence of wind. For those days the minimum water level is subtracted from the maximum after determination of relative zero level by averaging water levels within a day. Analysis results show that the water level rose twice a day due to the astronomical tide. This is called semi-diurnal tide with a tidal period of almost 12 hours. In Figure 5.8, the semi diurnal tide characteristics of the daily water level measured in Bostanli are shown.

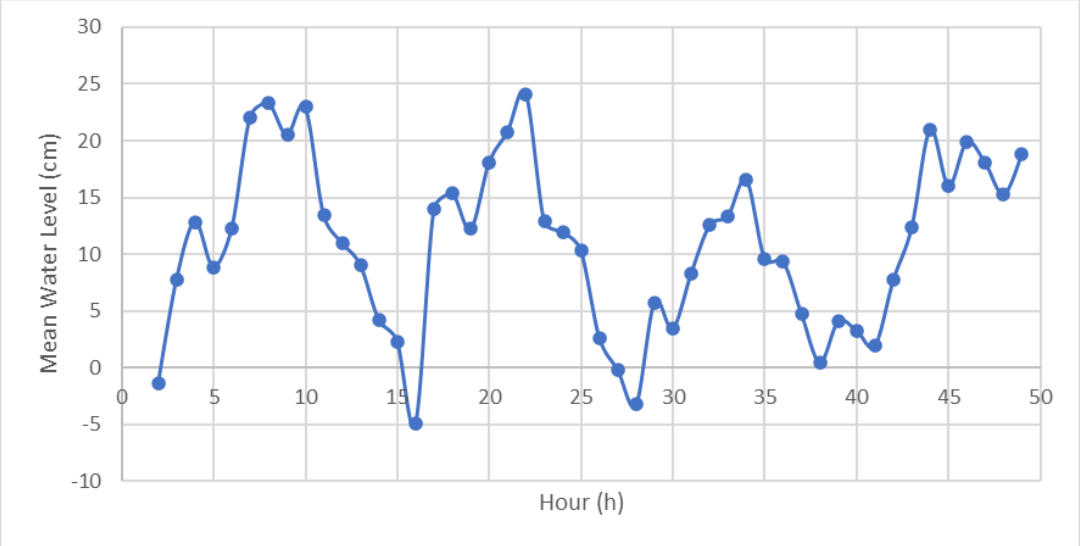

Figure 5.8. Semi-diurnal characteristics of daily tide measured in Bostanli measurement

As can be seen in Figure 5.8, sea-level change due to astronomical tide is generally between 10-40 cm. When the water level change is higher than 40 cm., it seems that there is a storm.

5.5. Seasonal Variation

Seasonal variation is the changes in sea level throughout the year. They affect oceanographic (ocean currents, etc.), hydrological (surface and groundwater flows) and meteorological (air pressure, precipitation, wind, evaporation, etc.) conditions.

In this study, seasonal water level changes were examined separately using each TUDES, Bostanli and Pasaport data. Figure 5.9, Figure 5.10 and Figure 5.11 show

seasonal water level changes with Bostanli, Pasaport and TUDES data, respectively. The graphs are plotted with the data of each year, showing the average monthly sea water level. The blue lines represent each year data, while the red line represents the overall average.

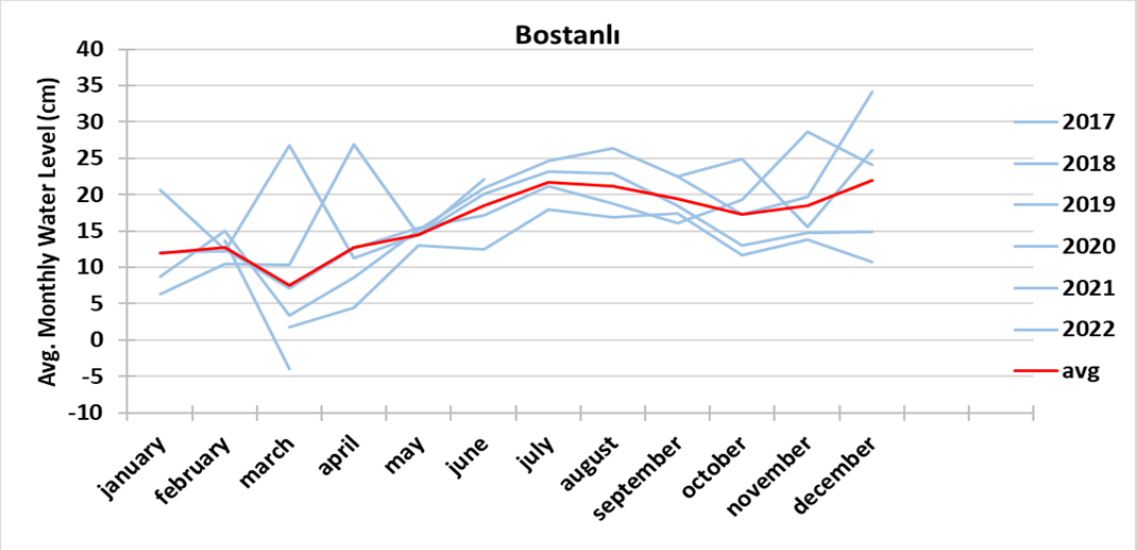

Figure 5.9. Monthly average water levels of Bostanli data by years (blue lines) and the overall average values (red line)

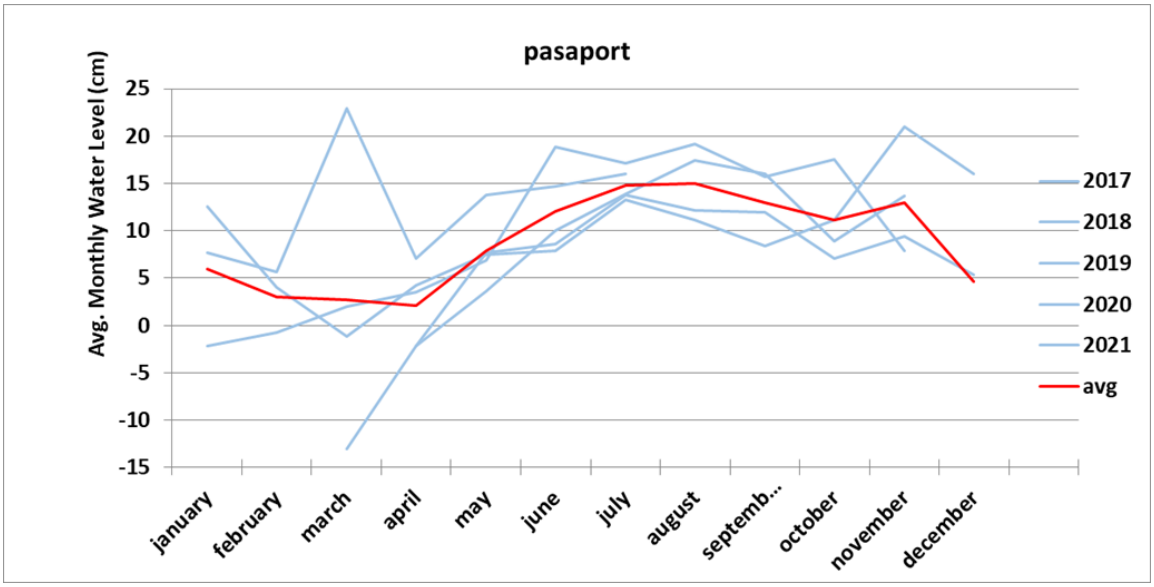

Figure 5.10. Monthly average water levels of Pasaport data by years (blue lines) and the overall average values (red line)

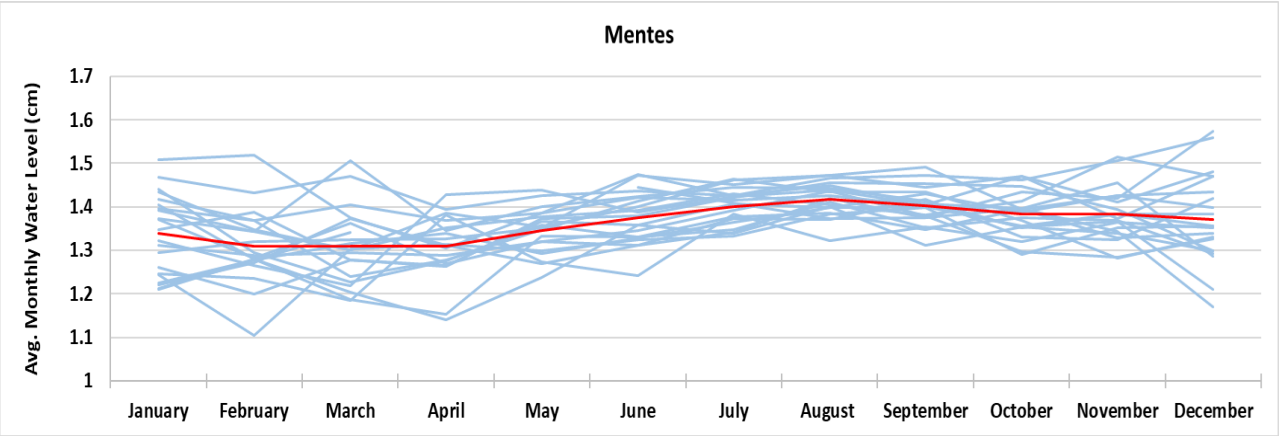

Figure 5.11. Monthly average water levels of TUDES data by years (blue lines) and the overall average values (red line)

Figures 5.9, 5.10 and 5.11 show that the water level decreases in winter season and increases in summer season. The difference between the maximum and the minimum sea water level gives the seasonal change and it is calculated as 22 cm, 21 cm and 24 cm for TUDES. Bostanli and for Pasaport dataset, respectively.

5.6. Climate Change Effect (Trendline)

With a temperature change, there is a global water level change in ocean water levels caused by the freezing and melting of polar ice caps and the thermal contraction and expansion of the ocean water body (Kamphius, 2020). With climate change, sea water level changes over many years.

One of the biggest problems of the world in the 21st century is global warming. Global warming has had many effects on the world order, one of which is climate change. The melting of glaciers as a result of climate change has caused an increase in sea water level. This increase is likely to threaten many coastal cities in the future. (Woodworth, 2006, IPCC, 2007).

In this section, the sea level trend is examined. Long data sets are needed when performing trend analysis. Since it would not be correct to make a trend analysis of 5-year data provided by Izmir Municipality, 21-year sea water level data of mareograph station in Mentes were used in this study. From an engineering point of view, it would be correct to find the normalized trends for trend analysis (Aydoğan & Ayat, 2018). Each

sea level value was normalized by dividing by the mean value of the series. The equation for normalization;

$$SWL^{*}_{k,t} = \frac{SWL^{k,t}}{SWL^{k}_{avg}} \quad (15)$$

where; $SWL^{*}_{k,t}$ is normalized sea water level, $SWL^{k,t}$ = Sea water level,

k= the number of network nodes,

t= time step,

SWL^{k}_{avg}= the mean of the series.

Various parametric or non-parametric methods can be used for trend analysis. While the data sets are normally distributed and independent in the parametric trend determination method, independent data sets are used in the non-parametric trend estimation method. Two non-parametric methods were used for trend estimation. These are the line of best fit and Theil-Sen estimator methods. The Mann-Kendall test was used to analyze the significance of the trends.

5.6.1. The Line of Best Fit

The line of best fit method is a method used for estimating non-parametric trend analysis. Time series equation of normalized sea water levels in a linear trend is given below;

$$NSWL = dt + e \quad (16)$$

where; NSWL is the normalized sea water level at a time instant,

d and e are regression parameters.

The d parameter specifies the trend size of the data. The equation for estimating d is given in Eq. 17;

$$d = \frac{\sum_{i=1}^{n}(NSWL_i - \overline{NSWL})(t_i - \bar{t})}{\sum_{i=1}^{n}(t_i - \bar{t})^2} \quad (17)$$

where; $\overline{NSWL}$= the mean of normalized seawater level

$\bar{t}$= the mean of the time series

The e parameter is the interception expression and it is defined as;

$$e = \overline{NSWL} - d\bar{t} \quad (18)$$

5.6.2. Theil-Sen Estimator

The Theil-Sen estimator is a popular non-parametric method used to estimate linear slope in non-parametric statistics (El-Shaarawi & Piegorsch ,2001). In this method, both slope and interception can be calculated as in the line of best fit method. To calculate the slope, Eq. 19 is used:

$$T_k = \frac{NSWL_j - NSWL_i}{t_j - t_i} \qquad \text{for k=1,2, …, N} \tag{19}$$

T_k is the slope of the kth term in the dataset, $NSWL_j$ and $NSWL_i$ are the normalized seawater level at time t_j and t_i, respectively. N is the number of data pairs. It is found as follows;

$$N = \frac{n(n-1)}{2} \tag{20}$$

where, n is data number.

The Theil-Sen trend estimate is the median of the T_k values. From the smallest to the largest T_k values, the Theil-Sen slope is found as follows;

$$T_m = \begin{cases} T_{[(N+1)/2]} & if \quad N\ is\ odd \\ \frac{T_{[N/2]} + T_{[(N+2)/2]}}{2} & if \quad N\ is\ even \end{cases} \tag{21}$$

The plus and minus values of T_m indicate the increase and decrease of the slope, while its value indicates the steepness of the slope.

5.6.3. Confidence Interval (CI)

Confidence interval was determined for the Theil-Sen estimator. confidence interval, s calculated by using Eq. 22,23 and 24.

$$SD = \sqrt{(Var(S))} \tag{22}$$

$$T_{m+CI} = T_s\left(\frac{n + SD * z_{1-\frac{\alpha}{2}}}{2}\right) \tag{23}$$

$$T_{m-CI} = T_s\left(\frac{n - SD * z_{1-\frac{\alpha}{2}}}{2}\right) \tag{24}$$

Ts(i) is the i^{th} term from the T_k values previously ordered from smallest to largest. SD is the standard deviation of S, Z is the standard normal test statistic and $z_{(1-\alpha/2)}$ can be

found in the standard normal distribution table in Table 3.5. In this study, 95% confidence level (α=0.10) was calculated for CI. So, the value of $z_{(1-\alpha/2)}$ is 1.96. Tm-CI and Tm+CI represent the lower and upper limits of the confidence interval.

5.6.4. Mann-Kendall Test

The Mann-Kendall Test is a non-parametric test generally used in hydrological and meteorological data (Zhang et al., 2001; Yue et al., 2002). Unlike the line of best fit and Theil-Sen Estimator, Mann-Kendall is used to find the significance level of the trend. The equation for S value calculation;

$$S = \sum_{i=1}^{n-1} \sum_{j=i+1}^{n} sgn(NSWL_j - NSWL_i) \quad (25)$$

where, S is the test statistic value, n is the number of data. $NSWL_j$ and $NSWL_i$ are the normalized sea level at times t_j and t_i, respectively. $sgn(NSWL_j - NSWL_i)$ is found as follows;

$$sgn(NSWL_j - NSWL_i) = \begin{cases} +1 & for \ (NSWL_j - NSWL_i) > 0 \\ 0 & for \ (NSWL_j - NSWL_i) = 0 \\ -1 & for \ (NSWL_j - NSWL_i) < 0 \end{cases} \quad (26)$$

Variance of S is defined as given in Eq..27;

$$Var(S) = \frac{n(n-1)(2n+5) - \sum_{j=1}^{p} t_j(t_j-1)(2t_j+5)}{18} \quad (27)$$

p is the number of linked groups (for this study; p=0), t_j is the number of data points in the j^{th} attached group. Then Z transform is calculated as given below:

$$Z = \begin{cases} \frac{S-1}{\sqrt{Var(S)}} & for \quad S > 0 \\ 0 & for \quad S = 0 \\ \frac{S+1}{\sqrt{Var(S)}} & for \quad S < 0 \end{cases} \quad (28)$$

The positive and negative values of Z indicate the increase and decrease of the trend, respectively.

In order to decide that the calculated Z value (increasing or decreasing trend) is significant or not, confidence level corresponding to Z value is calculated. To find the Confidence Level, the α/2 value corresponding to the Z value was found from Table 3.5.

Then the confidence level is equal to 1- α, where α is specific significance level. If confidence level is higher than 50%, it means that the trend result is significant.

In this study, the trend of the mean and maximum sea water levels were examined using 21-year data of Mentes station. They were analyzed annually and monthly. In Figure 5.12 and Figure 5.13, trend graphs of mean and maximum sea water levels are shown, respectively. In these graphs, the line of best fit (d), Theil Sen's Median (T) and the Confidence Limits (T ± CI) trend lines are shown.

Table 5.1. Probabilities corresponding to the Z score

Z Tablosu

z	0	0.01	0.02	0.03	0.04	0.05	0.06	0.07	0.08	0.09
0.0	0.5000	0.4960	0.4920	0.4880	0.4840	0.4801	0.4761	0.4721	0.4681	0.4641
0.1	0.4602	0.4562	0.4522	0.4483	0.4443	0.4404	0.4364	0.4325	0.4286	0.4247
0.2	0.4207	0.4168	0.4129	0.4090	0.4052	0.4013	0.3974	0.3936	0.3897	0.3859
0.3	0.3821	0.3783	0.3745	0.3707	0.3669	0.3632	0.3594	0.3557	0.3520	0.3483
0.4	0.3446	0.3409	0.3372	0.3336	0.3300	0.3264	0.3228	0.3192	0.3156	0.3121
0.5	0.3085	0.3050	0.3015	0.2981	0.2946	0.2912	0.2877	0.2843	0.2810	0.2776
0.6	0.2743	0.2709	0.2676	0.2643	0.2611	0.2578	0.2546	0.2514	0.2483	0.2451
0.7	0.2420	0.2389	0.2358	0.2327	0.2297	0.2266	0.2236	0.2207	0.2177	0.2148
0.8	0.2119	0.2090	0.2061	0.2033	0.2005	0.1977	0.1949	0.1922	0.1894	0.1867
0.9	0.1841	0.1814	0.1788	0.1762	0.1736	0.1711	0.1685	0.1660	0.1635	0.1611
1.0	0.1587	0.1563	0.1539	0.1515	0.1492	0.1469	0.1446	0.1423	0.1401	0.1379
1.1	0.1357	0.1335	0.1314	0.1292	0.1271	0.1251	0.1230	0.1210	0.1190	0.1170
1.2	0.1151	0.1131	0.1112	0.1094	0.1075	0.1057	0.1038	0.1020	0.1003	0.0985
1.3	0.0968	0.0951	0.0934	0.0918	0.0901	0.0885	0.0869	0.0853	0.0838	0.0823
1.4	0.0808	0.0793	0.0778	0.0764	0.0749	0.0735	0.0721	0.0708	0.0694	0.0681
1.5	0.0668	0.0655	0.0643	0.0630	0.0618	0.0606	0.0594	0.0582	0.0571	0.0559
1.6	0.0548	0.0537	0.0526	0.0516	0.0505	0.0495	0.0485	0.0475	0.0465	0.0455
1.7	0.0446	0.0436	0.0427	0.0418	0.0409	0.0401	0.0392	0.0384	0.0375	0.0367
1.8	0.0359	0.0352	0.0344	0.0336	0.0329	0.0322	0.0314	0.0307	0.0301	0.0294
1.9	0.0287	0.0281	0.0274	0.0268	0.0262	0.0256	0.0250	0.0244	0.0239	0.0233
2.0	0.0228	0.0222	0.0217	0.0212	0.0207	0.0202	0.0197	0.0192	0.0188	0.0183
2.1	0.0179	0.0174	0.0170	0.0166	0.0162	0.0158	0.0154	0.0150	0.0146	0.0143
2.2	0.0139	0.0136	0.0132	0.0129	0.0126	0.0122	0.0119	0.0116	0.0113	0.0110
2.3	0.0107	0.0104	0.0102	0.0099	0.0096	0.0094	0.0091	0.0089	0.0087	0.0084
2.4	0.0082	0.0080	0.0078	0.0076	0.0073	0.0071	0.0070	0.0068	0.0066	0.0064
2.5	0.0062	0.0060	0.0059	0.0057	0.0055	0.0054	0.0052	0.0051	0.0049	0.0048
2.6	0.0047	0.0045	0.0044	0.0043	0.0042	0.0040	0.0039	0.0038	0.0037	0.0036
2.7	0.0035	0.0034	0.0033	0.0032	0.0031	0.0030	0.0029	0.0028	0.0027	0.0026
2.8	0.0026	0.0025	0.0024	0.0023	0.0023	0.0022	0.0021	0.0021	0.0020	0.0019
2.9	0.0019	0.0018	0.0018	0.0017	0.0016	0.0016	0.0015	0.0015	0.0014	0.0014
3.0	0.0014	0.0013	0.0013	0.0012	0.0012	0.0011	0.0011	0.0011	0.0010	0.0010
3.1	0.0010	0.0009	0.0009	0.0009	0.0008	0.0008	0.0008	0.0008	0.0007	0.0007
3.2	0.0007	0.0007	0.0006	0.0006	0.0006	0.0006	0.0006	0.0005	0.0005	0.0005
3.3	0.0005	0.0005	0.0005	0.0004	0.0004	0.0004	0.0004	0.0004	0.0004	0.0004
3.4	0.0003	0.0003	0.0003	0.0003	0.0003	0.0003	0.0003	0.0003	0.0003	0.0002
3.5	0.0002	0.0002	0.0002	0.0002	0.0002	0.0002	0.0002	0.0002	0.0002	0.0002
3.6	0.0002	0.0002	0.0002	0.0001	0.0001	0.0001	0.0001	0.0001	0.0001	0.0001
3.7	0.0001	0.0001	0.0001	0.0001	0.0001	0.0001	0.0001	0.0001	0.0001	0.0001
3.8	0.0001	0.0001	0.0001	0.0001	0.0001	0.0001	0.0001	0.0001	0.0001	0.0001
3.9	0.0001	0.0001	0.0000	0.0000	0.0000	0.0000	0.0000	0.0000	0.0000	0.0000
4.0	0.0000	0.0000	0.0000	0.0000	0.0000	0.0000	0.0000	0.0000	0.0000	0.0000

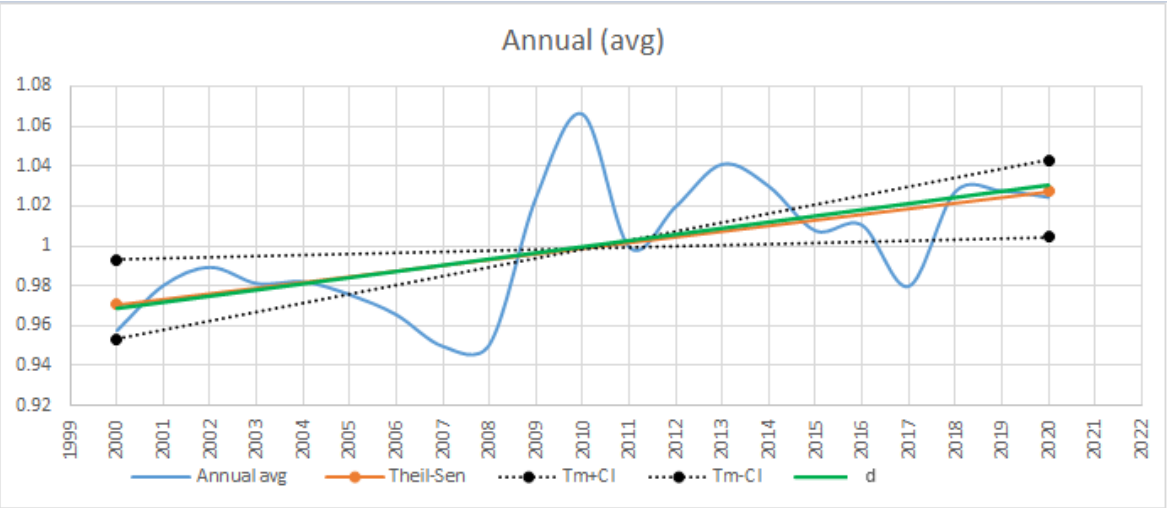

Figure 5.12. Annual average NSWL trend graph

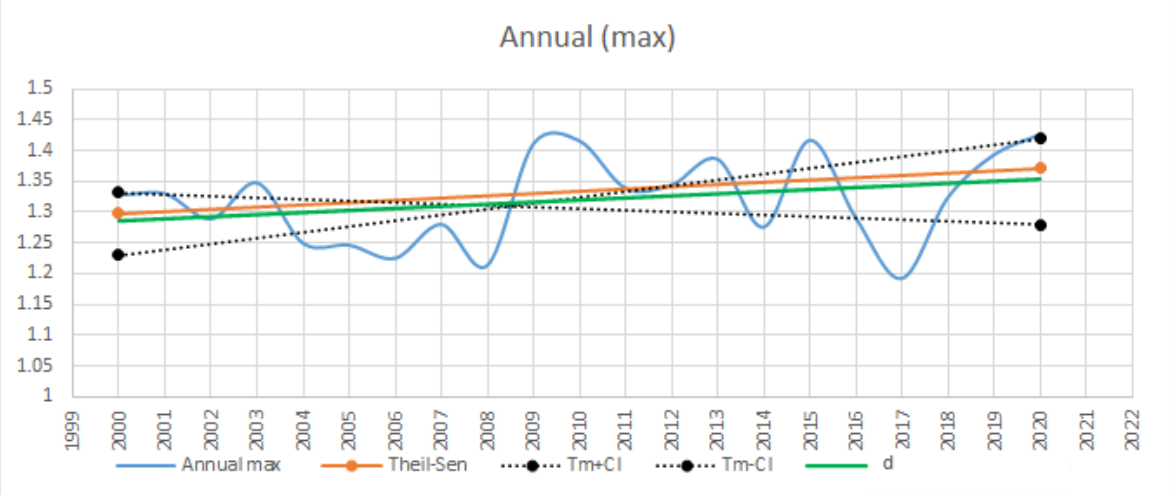

Figure 5.13. Annual maximum NSWL trend graph

As seen in Figure 5.12 and Figure 5.13, there is an increasing trend in both annual average and maximum sea water levels. According to the Theil-Sen estimator, there is an increase trend of 0.284 %/year for the average sea water level and 0.367 %/year for the maximum sea water level. According to the line of best fit, it tends to increase by 0.307 %/year for the average and 0.332 %/year for the maximum sea water level. In Table 5.2 and Table 5.3, trend analysis results are given annually and monthly for the average and max sea water levels, respectively given. In these tables, the line of best fit slope (d), Theil-Sen estimator(T), the upper (Tm+CI) and lower (Tm-CI) Confidence Intervals of Theil Sen estimator, the Z value of Mann-Kendall test and confidence level and trend tendency according to Mann-Kendall methods are given. Since the trend analysis is done

according to the normalized data, it would be more appropriate to examine the calculated trends as %/year (Aydoğan & Ayat, 2018).

Table 5.2. Trend analysis results for the average sea water level.

	T (%/year)	Tm+CI (%/year)	Tm-CI (%/year)	d (%/year)	Z	Confidence Level (%)	Trend Direction
Annual	0.284	0.449	0.056	0.307	2.325	97.993	Increasing
January	0.263	0.843	-0.304	0.292	0.876	61.897	Increasing
February	0.303	0.591	-0.122	0.334	1.419	84.41	Increasing
March	0.429	0.836	-0.093	0.405	1.721	91.475	Increasing
April	0.224	0.4	-0.39	0.256	0.941	65.33	Increasing
May	0.356	0.498	0.023	0.381	2.498	98.751	Increasing
June	0.482	0.721	0.28	0.511	3.412	99.936	Increasing
July	0.291	0.478	0.154	0.341	2.688	99.281	Increasing
August	0.285	0.455	0.09	0.281	2.748	99.4	Increasing
September	0.228	0.412	-0.037	0.219	1.842	93.452	Increasing
October	0.284	0.552	-0.086	0.261	1.6	89.04	Increasing
November	0.242	0.575	-0.108	0.288	1.721	91.475	Increasing
December	0.154	0.697	-0.551	0.194	0.513	39.205	No Trend

Table 5.3. Trend analysis results for the maximum sea water level.

	T (%/year)	Tm+CI (%/year)	Tm-CI (%/year)	d (%/year)	Z	Confidence Level (%)	Trend Direction
Annual	0.367	0.942	-0.258	0.332	6.311	100.00	Increasing
January	0.373	1.2	-0.469	0.341	-3.654	99.97	Decreasing
February	0.386	0.871	-0.456	0.345	3.835	99.99	Increasing
March	0.596	1.228	-0.027	0.632	4.922	100.00	Increasing
April	0.263	0.629	-0.59	0.294	1.914	94.44	Increasing
May	0.353	0.55	-0.336	0.377	2.304	97.88	Increasing
June	0.584	0.854	0.174	0.53	5.707	100.00	Increasing
July	0.308	0.49	0.08	0.34	5.405	100.00	Increasing
August	0.304	0.513	0.021	0.319	4.016	99.99	Increasing
September	0.192	0.44	-0.067	0.251	5.345	100.00	Increasing
October	0.418	0.853	-0.062	0.339	3.11	99.81	Increasing
November	0.161	0.602	-0.366	0.161	-3.714	99.98	Decreasing
December	0.228	1.062	-0.464	0.399	6.311	100.00	Increasing

Confidence level is considered as no trend if it is below 50%. As can be seen in Table 5.2 and Table 5.3, the confidence level values are more than 50% except month December of the average sea water level. Although there is an increasing trend in the

average water level for all the months (except no trend case in December), there is a decreasing trend in January and November for the maximum sea water level.

When the trend analysis was performed with normalized sea water levels obtained from the mareograph station at TUDES Mentes location, it was observed that the sea water level was increasing. When the trend was examined with Theil-Sen and the line of best fit techniques, an increase is observed in all months and annual., trends were tested and their reliability was checked using Mann-Kendall test. Mann-Kendall test showed that the calculated increasing trends for the mean water level and the maximum water level are reliable. However, while Theil-Sen and the line of best fit method gave increasing trend for January and November, Mann-Kendall estimated a decreasing trend. The annual increase rate of sea water level is 0.284 %/year and 0.306 %/year according to Theil-Sen estimator and the line of best fit method, respectively. It means that if the water depth is 2m, it may rise 28.4% in 100 years and reach to 2.57m and 2.61m according to Theil-Sen and the line of best fit estimation methods, respectively.

CHAPTER 6

WAVE MODELING

The primary agents impacting the stability of coastal structures, altering the coastline, and generating coastal flooding are sea waves. Therefore, no engineering project can be performed without knowledge of the wave characteristics at a location.

Instrumental in-situ wave measurements are one of the most reliable means of determining wave conditions at a location. Although certain practical difficulties are involved with instrumental measurements, such as the loss of data and equipment or their expensive cost, measurement campaigns can often be planned to get trustworthy wave data for engineering applications and confirm modeling conclusions (Bilyay et al., 2011).

In the absence of in-situ wave measurement data, like in the case of Izmir, numerical model estimates are often used because of their broad temporal and geographical coverage and lower cost. In this study, waves are modeled using a third-generation nearshore wave model, SWAN (Simulating Waves Nearshore), which is driven by the most recent re-analysis of offshore wind data called ERA5 from the European Centre for Medium-Range Weather Forecasts (ECMWF). To simulate nearshore waves, the SWAN Cycle III v.41.20 model is executed in the two-dimensional non-stationary mode. The SWAN model represents the effects of generation, spatial propagation, refraction, shoaling, dissipation, and nonlinear wave-wave interactions. It is a third-generation, fully-spectral model that solves the spectral action balance equation. (SWAN group, 2017) Since SWAN calculates wave propagation from deep water to the surf zone, it is appropriate to use it in coastal areas.

The evolution of the wave spectrum is described by the spectral action balance equation, which, for Cartesian coordinates, is [e.g., Hasselmann et al., 1973].

$$\frac{\partial N}{\partial t} + \nabla_{\vec{x}}[(\overrightarrow{c_g} + \vec{U})N] + \frac{\partial C_\sigma N}{\partial \sigma} + \frac{\partial C_\theta N}{\partial \theta} = \frac{S_{tot}}{\sigma} \qquad (29)$$

where; N is the action density defined as N = E/σ. E is the energy density, as a function of the frequency σ and propagation direction θ.

The first term on the left-hand side of Eq. (2.7) represents the local rate of change of action density in time. The second and third term represents the propagation of action in geographical space (with propagation velocities cx and cy in x and y space, respectively). The fourth term describes shifting of the relative frequency due to

variations in depths and currents (with propagation velocity cσ in σ space). The fifth term represents depth-induced and current-induced refraction (with propagation velocity cθ in θ space). The term S [=S(σ,θ)] at the right-hand side of the action balance equation is the source/sink term in terms of energy density, representing the effects of generation, dissipation, and nonlinear wave-wave interactions.

The SWAN model was run in non-stationary and stationary mode. it was run in stationary mode when using extreme wind data. The number of directions is 36, resulting in a direction resolution of =10 degrees for the wind sea. 33 discretization frequencies exist between the lowest (0.043 Hz) and the highest (1.0 Hz) frequencies in the SWAN model. This suggests that the periods of the simulated waves range from 1 to 23 seconds. For white-capping, the equation suggested by Janssen with the coefficient Cds=1 is used. According to Battjes and Janssen (1978), the proportionality coefficient =1 and the breaker index =0.73 are used to describe depth-limited wave breaking. Zijlema et al. (2012) utilize the empirical JONSWAP model of Hasselmann et al. (1973) with CJON = 0.038 m^2s^{-3} for bottom friction.

The bathymetry file has been edited in order to work in a smaller area with a lower resolution. It is set to be 26 km in the x direction and 9.85 km in the y direction. There are 5250 and 1978 grids with 5 m interval in x and y direction, respectively. The same grid system is also used for the computations.

The input file of the SWAN model is shown in Figure 6.1. For more detailed information, see the SWAN USER MANUAL.

```
$12345678901234567890123456789012345678901234567890123456789012345678901
$*************************************************************************
$
PROJ 'test' '01' 'izmir3-k.swn'                                          &
$
$ using SWAN 40.91
$
$************* MODEL INPUT ***********************************************
$
SET level=1 depmin = 0.5  maxmes = 9  maxerr = 3
$
SET pwtail = 4
$
SET nor=90.0 NAUT
$
CGRID REGULAR xpc = 0   ypc = 0     alpc = 0.                    &
            xlenc = 26250  ylenc = 9850                            &
              mxc = 525      myc =197                              &
      CIRCLE                                                       &
              mdc = 36                                             &
              fhigh = 1.0  msc = 33
$
INPGRID BOTTOM xpinp = 0   ypinp = 0   alpinp = 0.             &
               mxinp = 5250     myinp = 1978                       &
               dxinp = 5.     dyinp = 5.                        &
               EXCEPTION excval = -25
READINP BOTTOM  fac=1.                                             &
 'korfez-k-5.r2s'  idla = 4  nhedf = 19  FREE
$
INPGRID WIND   xpinp = 0   ypinp = 0  alpinp = 0.              &
               mxinp = 110       myinp = 74                        &
               dxinp = 239.    dyinp = 134.                      &
READINP WIND  fac=1.0                                             &
 'windfieldSSE-29-max.txt'  idla = 4  nhedf = 0  FREE
$
$************* PROPAGATION / DISSIPATION *********************************
GEN3 KOMEN AGROW
WCAPping JANSSEN cds1=1 delta=1
QUADrupl
BREaking constant alpha=1.0 gamma=0.73
FRICTION JONSWAP 0.038
TRIAD trfac=0.10 cutfr=2.5
LIMITER ursell=10 qb=1.0
PROP BSBT
$
$************* NUMERICAL SETTINGS ****************************************
$
NUM STOPC drel = 0.01  curvat = 0.01                               &
    npnts = 98.  STAT mxitst = 40
$
$************* OUTPUT REQUESTS *******************************************
$
$ Other outputs ------------------------------------------------------
$
TABLE 'COMPGRID' HEADER 'izmir-k-SSE-29-max.out' XP YP BOTLEV DEP HSIGN        &
             TM02 TMM10 TPS DIR WIND

$
COMPUTE
STOP
```

Figure 6.1. Swan input file used in the modeling

In this study, only wind input is used in the SWAN model. Sample wind input file with the x and y components of wind velocity is given in Figure 6.2. In this example x component of the wind velocity is -2.73m /s and y component is 18.55 m/s. SWAN can understand the wind direction from x and component of the wind velocity as tan (u_y/u_x)

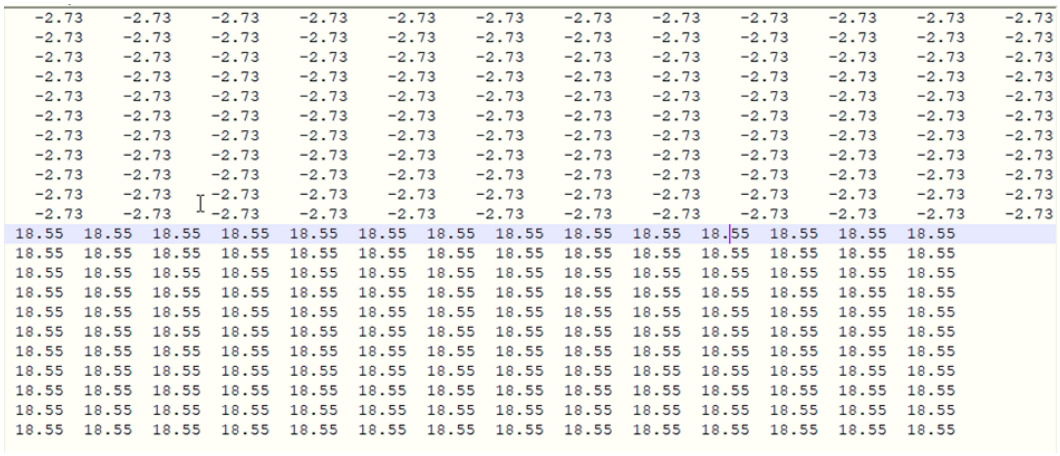

Figure 6.2. Wind file for SWAN

The model is asked to output the results for the time, X and Y coordinates, bottom elevation, water depth, significant wave height (H_s), wave periods T_{m02}, T_{m010}, and T_p, wave direction parameters, and wind speed. The average height of the highest one-third of the waves is the significant wave height. Since SWAN is a spectral model, it calculates the wave height obtained from the spectrum called as H_{m0}. However, since it is assumed that $H_s = H_{m0}$, it is also called as the significant wave height. From the zeroth and second spectral moments, T_{m02} is the mean wave period, T_{m010} is the wave energy period, and T_p is the peak wave period corresponding to the spectral peak.

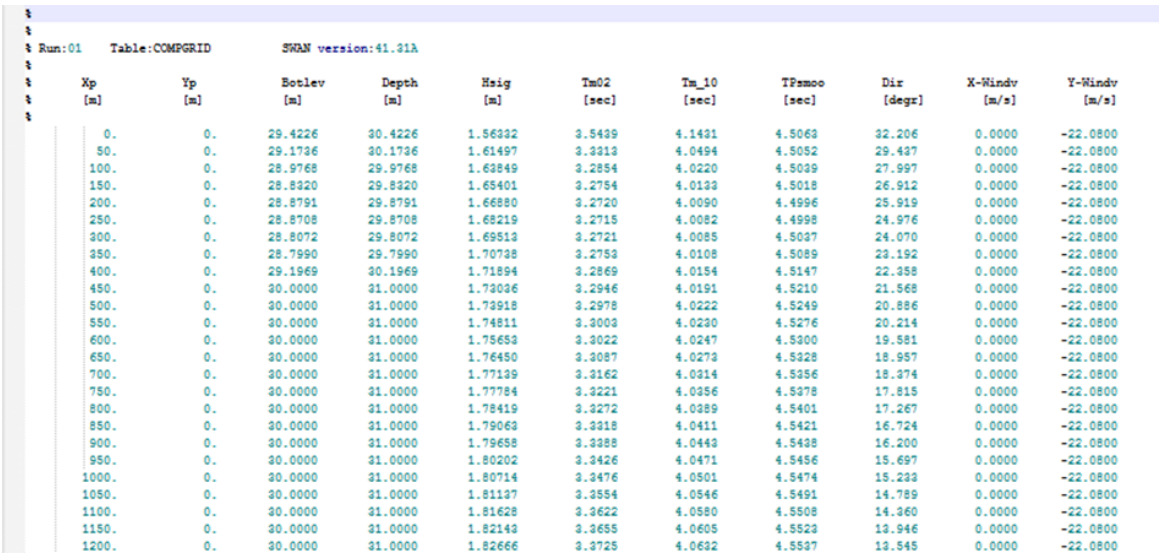

Figure 6.3. An example of a SWAN output file

SWAN gives the output as a text file. In order to visualize the outputs on the study area, the software Blue Kenue is used. However, output file must be converted to r2s and r2v files to visualize the results in Blue Kenue. SWANMangler _v3.1 software is used for this conversion. Run of SWANMangler _v3.1 software is shown in Figure 6.4.

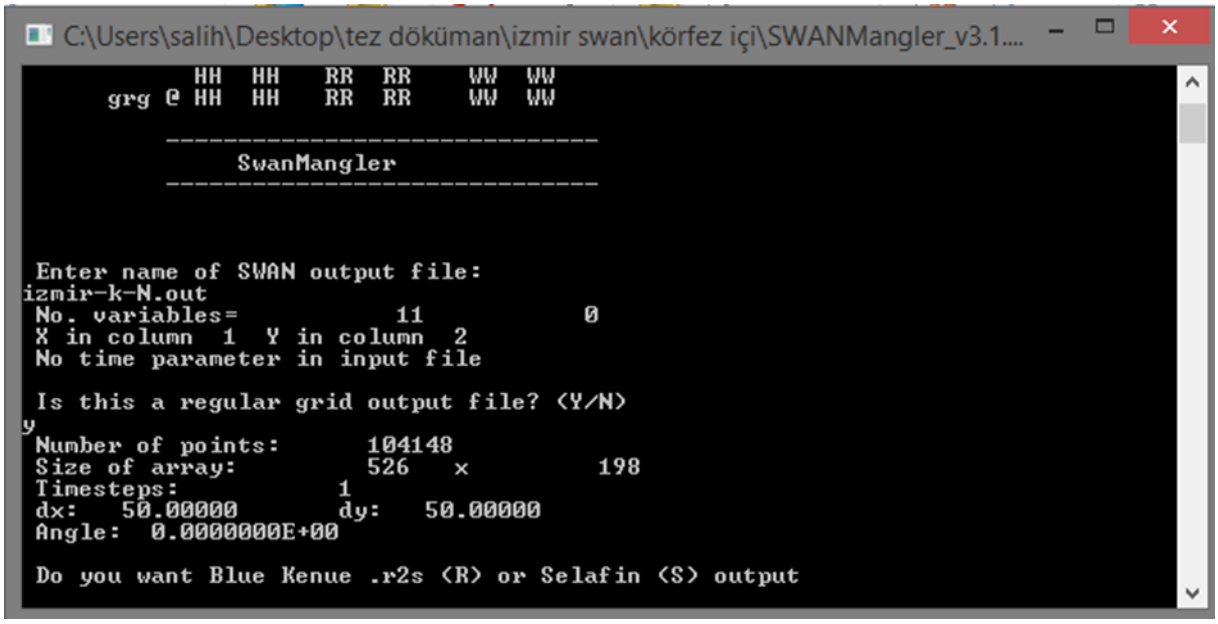

Figure 6.4. SWANMangler_v3.1 software

The model is executed for the following directions: N, NNW, NW, WNW, W, WSW, SW, SSW, S, SSE, and SE. Figure 6.5 shows the model results on the study area (inner bay)

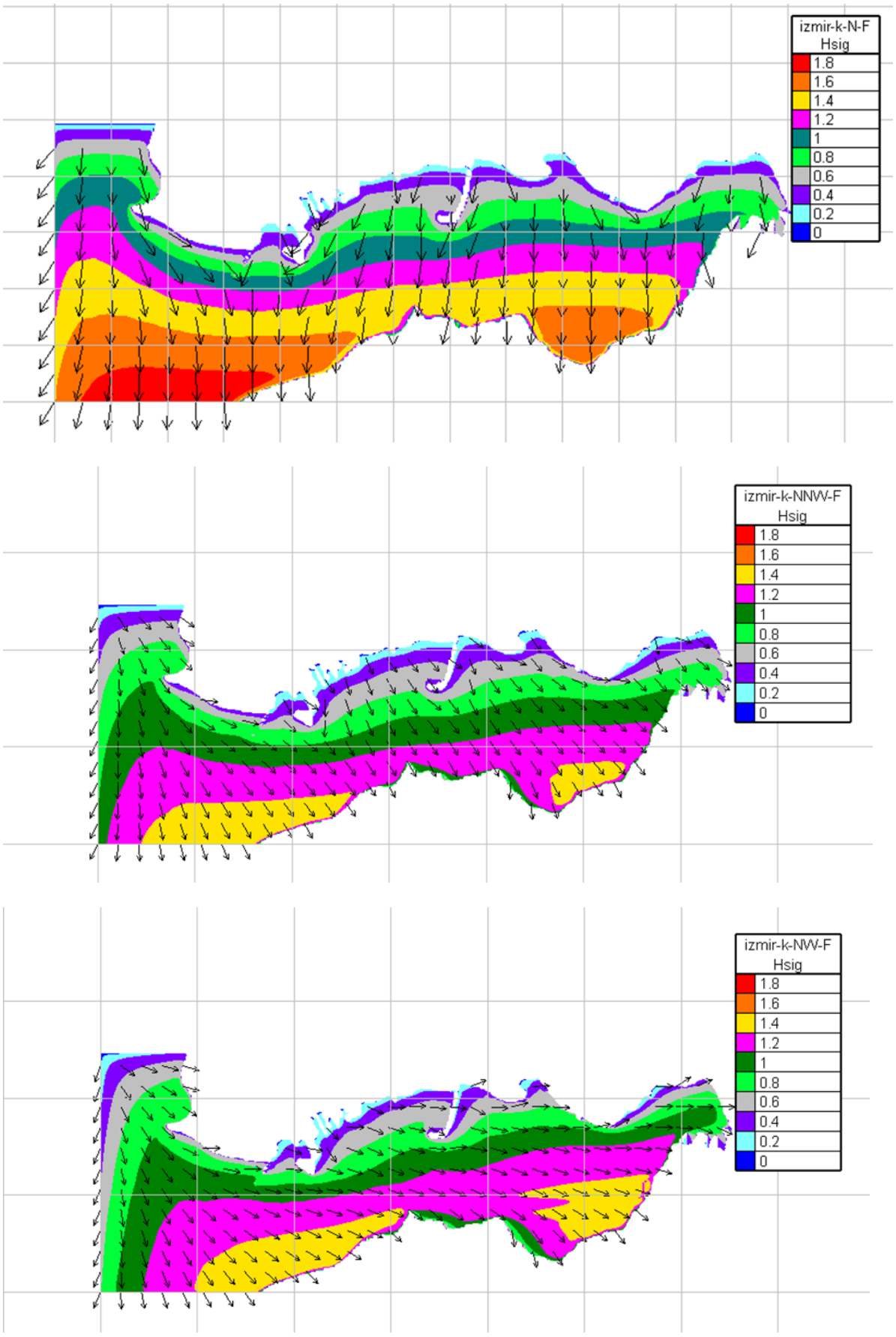

Figure 6.5. (Cont. on next page)

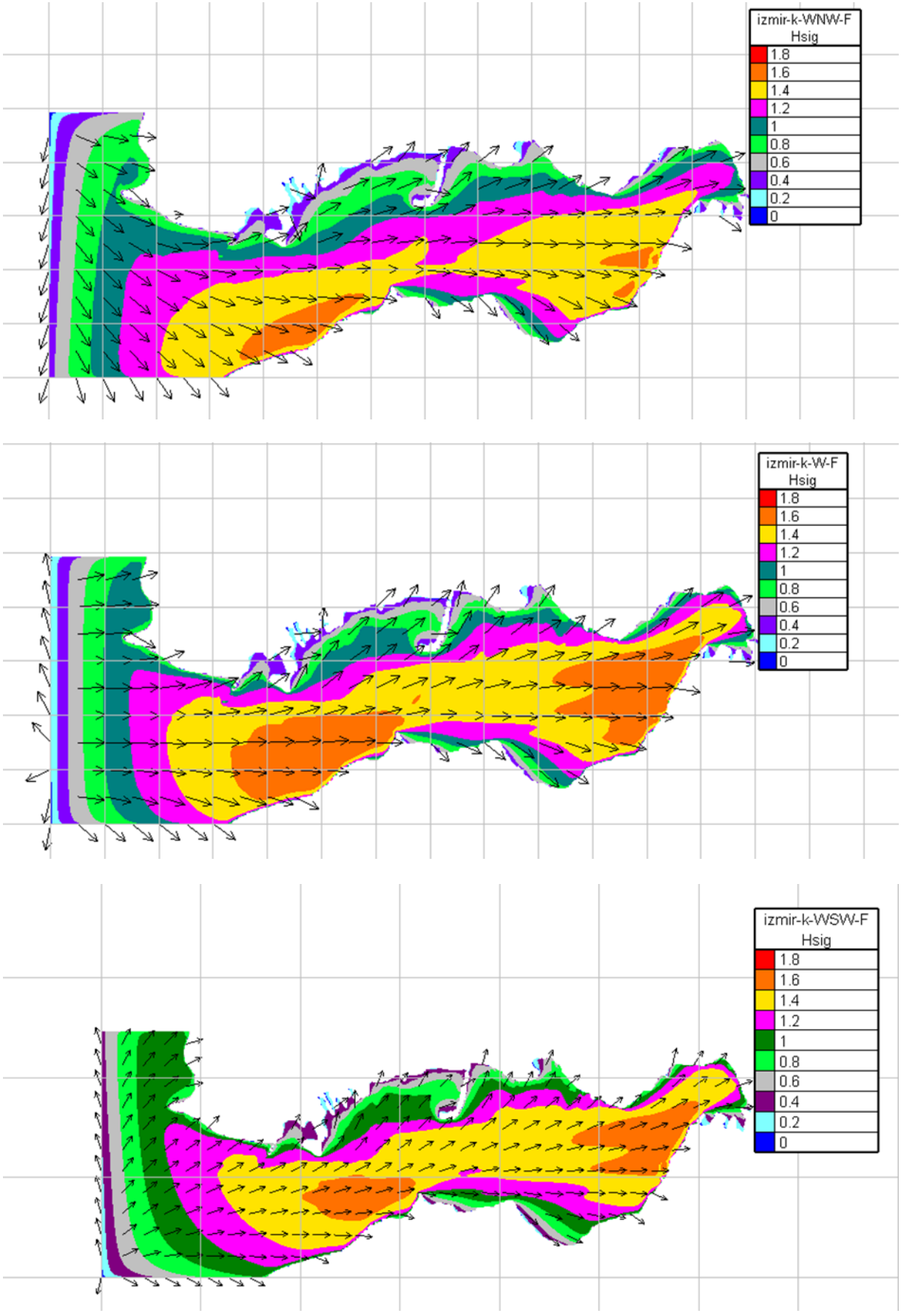

Figure 6.5. (Cont. on next page)

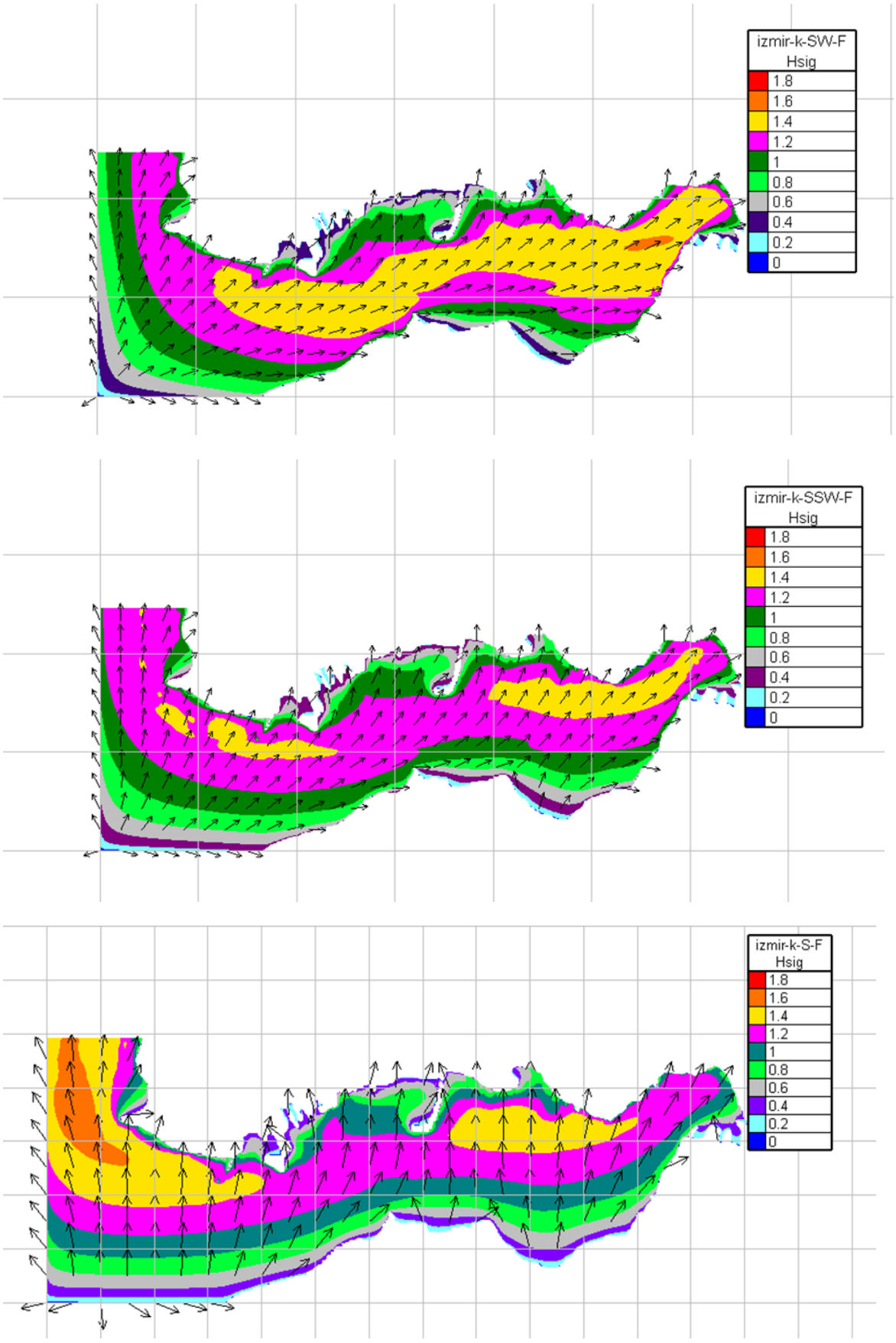

Figure 6.5. (Cont. on next page)

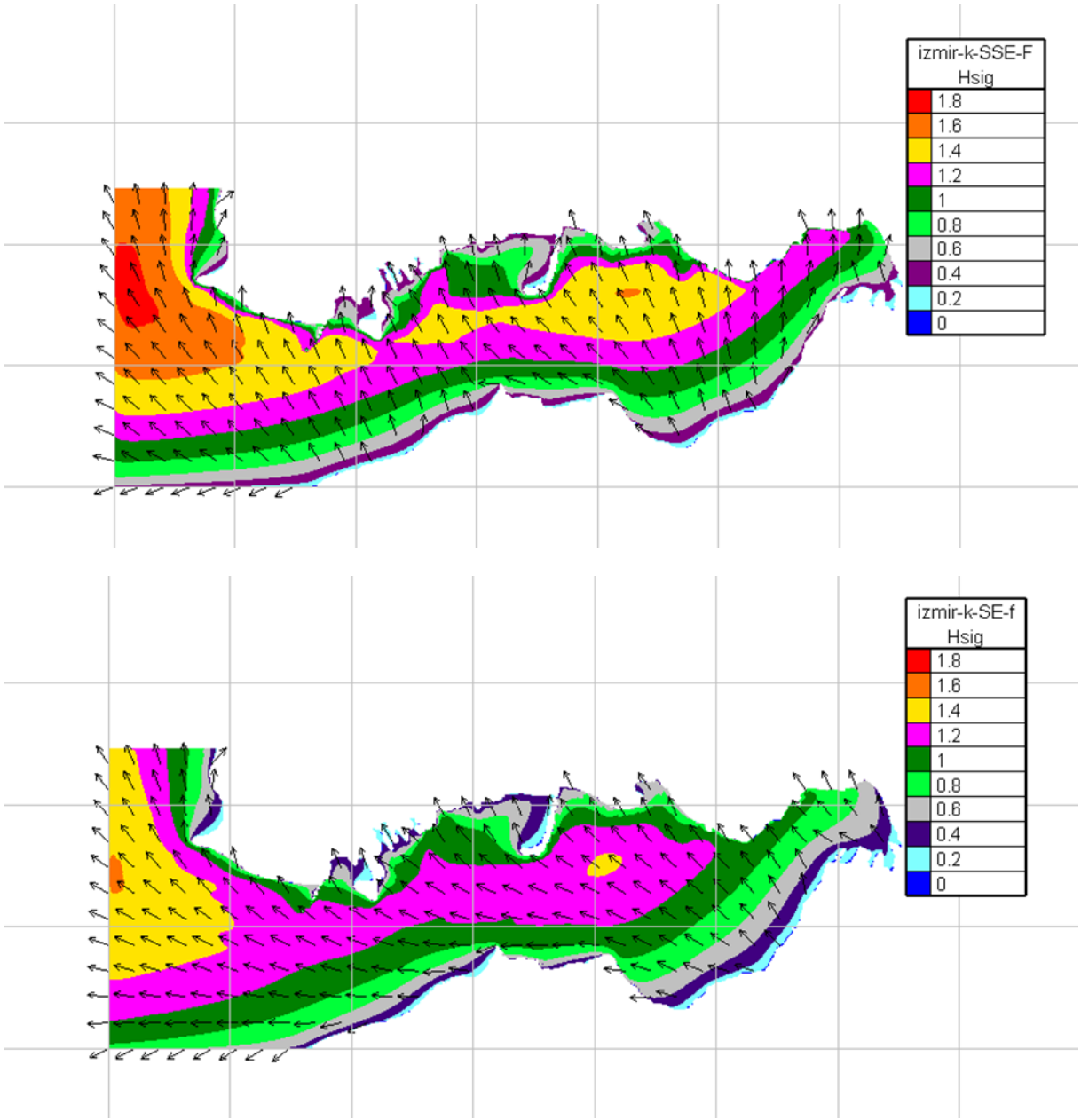

Figure 6.5. SWAN Wave model results for the wave height corresponding to different directions

Considering the model results given in Figure 6.5, vulnerable areas in Izmir Bay from the coastal flood side of view are determined and shown in Figure 6.6.

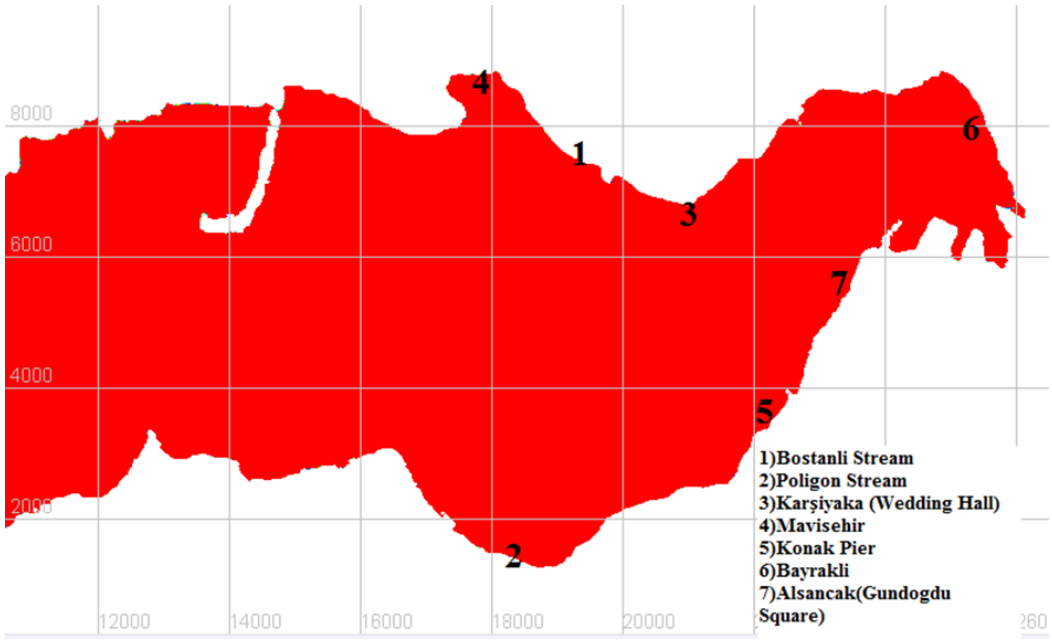

Figure 6.6. Vulnerable Coasts associated with risk of flooding in Izmir Bay

In Table 6.1, the wave heights are given for the various directions found for the critical areas in the model.

Table 6.1. Wave heights for various directions

	NNW	NW	WSW	SW	SSW	SSE	SE	N	S	W	WNW
Bostanli	0.598	0.829	1.123	1.140	1.130	1.109	0.913	0.496	1.130	1.083	0.988
Poligon	1.146	1.007	0.547	0.342	0.231	0.357	0.468	1.457	0.244	0.752	0.891
Karsiyaka	0.587	0.857	1.194	1.203	1.183	1.153	0.984	0.541	1.170	1.168	1.063
Mavisehir	0.224	0.340	0.649	0.692	0.715	0.759	0.701	0.253	0.742	0.588	0.497
Konak	1.224	1.317	1.284	1.098	0.821	0.390	0.251	1.286	0.574	1.425	1.406
Bayrakli	0.535	0.831	1.218	1.201	1.120	0.786	0.465	0.382	0.989	1.197	1.073

Wave heights in those critical areas are determined using the SWAN model results given in Figure 6.5. The maximum wave heights which occurred in 7 critical areas are given in Table 6.2.

Table 6.2. The maximum wave heights and periods calculated using the SWAN model results in the critical areas

Locations	**Hs(m)**	**Tp(s)**
Bostanli	1,13	3,87
Poligon	1,46	4,16
Karsiyaka	1,17	4,62
Mavisehir	0,74	3,74
Konak	1,43	4,85
Bayrakli	1,20	4,77

CHAPTER 7

COASTAL FLOOD CALCULATIONS

During severe storms, sea level rises and large waves are formed. These waves in front of the coastal protection structures may exceed the upper elevation. This is called as wave overtopping and it may structure cause coastal flooding. Therefore, in order to determine the effect of coastal flooding, the amount of wave overtopping at these structures should be calculated. The coastline of İzmir is densely populated and economically important. In these regions with high fragility, the flood problem causes significant difficulties.

There are many models and techniques to calculate the amount of wave overtopping. In this study, Neural Network model developed by the Deltares team is used. Overtopping Neural Network model is derived from nearly 10000 physical model tests conducted in 11 countries (Steendam et al., 2004). Researches show that it can be used in the calculation of overtopping discharge for various coastal protection structures (Ozbahceci and Bilyay, 2018, Van Gent et al.,2007).

Overtopping Neural Network model is a user friendly model. The overtopping discharge can be calculated by entering the section properties and wave properties from the website https://www.deltares.nl/en/software/overtopping-neural-network/.It requires 15 parameters as input. In Figure 7.1, these parameters are shown on an example section and their explanations are given.

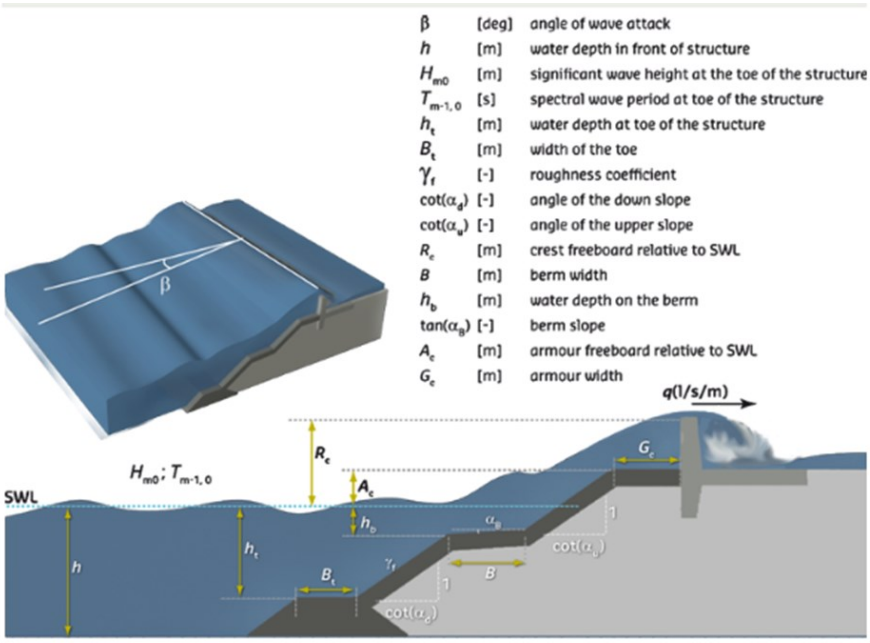

Figure 7.1. Parameters and explanations used for NN modeling of overtopping discharge in coastal structures (www.deltares.nl)

The screen where input parameters are entered appears in Figure 7.2.

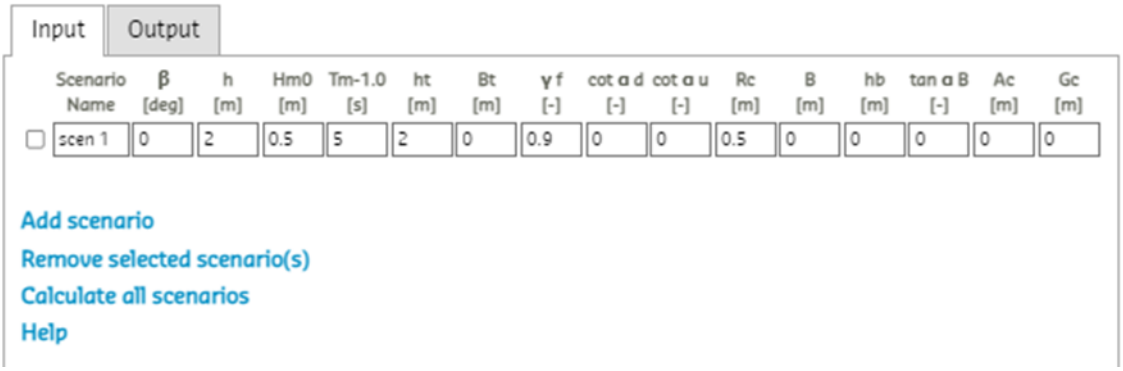

Figure 7.2. Parameters input screen of the Overtopping Neural Network model

There are 2 types of coastal protection structures along the Izmir Bay, namely the vertical sea walls and the rubble mound sloping revetments. In this study, 45 vertical sea wall and 42 rubble mound sloping revetments cross-sections along the Izmir Bay provided by Izmir Municipality are analyzed. Locations and codes of those sections are as follows;

-Bayrakli: S01, S02, S03, S04, S05, S06, S07, S08, S09, S22, S23, V05, V06, V07, V08, V09, V10, V11, V12, V13, V14, V15, V16, V17, V18, V19, V20

-Konak: S17, S18, S21, V21, V22, V23, V24, V25, V26, V27, C1, C2, C3, C4, C5, C6, C7

-Bostanli: V19, S10, S11, S12, S13, S14, S15, S16, S24, S25, S26

-Poligon: V28

-Karsiyaka: V01, V02, V03, V04, V29, V30, V31, V32, V33, V34, V35, V36, V37, V38

-Mavisehir: D-1, D-2, D-5, D-7, D-8, D-9, D-10, D-11, D-12, D-13, D-14, D-15, D-16, D-17, D-18, D-19, D-20, D-21.

where; S and D mean sloping type structure and V means vertical structure.

Although overtopping Neural Network model can be used for various structures, values of the parameters have some limitations. These limits are based on the H value. Figure 7.3, shows parameter limits for H=1m. In this study, the limit value is used if the parameters are outside the limit value. When the wave height is different than 1m, limiting value can be found using wave height ratio. For example, if the wave height is 1.5m, then the minimum and the maximum water depth to be entered in the model are 1.35m (1.5x0.9) and 30m (1.5x20).

1 m	<	H_{m0}	<	1 m
0.005	<	$s_{m-1,0}$	<	0.07
0	<	β	<	80
0.9 m	<	h	<	20 m
0.5 m	<	h_t	<	20 m
0	<	B_t	<	10 m
0.3	<	γ_f	<	1
0	<	$cot\ \alpha_d$	<	10
-1	<	$cot\ \alpha_u$	<	10
0	<	B	<	15 m
-1 m	<	h_b	<	5 m
0	<	$tan\ \alpha_B$	<	0.1
0.5 m	<	R_c	<	5 m
0	<	A_c	<	5 m
0	<	G_c	<	10 m

Figure 7.3. The available input parameters ranges of validity for the significant wave height of Hm0=1 m

7.1. Overtopping Discharge results for Vertical Sea Wall

Overtopping discharge is represented by q and it is calculated as mean discharge. It means that it is the overtopped volume divided by total duration and total width of the structure. Therefore its unit is lt/m.s or m^3/m.s.

There are 15 input parameters in Overtopping Neural Network model. In this study, 9 parameters are kept the same and 6 parameters are changed according to section dimensions and location for vertical sea walls. Parameters that are the same for all sections; β=0, Bt=0, γf=1, cot αd=0, cot αu=0, B=0, hb=0, tan αB=0, Gc=0.

Input values for vertical sea walls at current still water level and the calculated overtopping discharges are given in Table 7.1. Here, the wave height and wave period are taken from table Table 6.2 according to the section location.

Table 7.1. Input parameters and calculated overtopping discharge for vertical walls at current still water level

Name	h [m]	Hm0 [m]	Tm-1.0 [s]	ht [m]	Rc [m]	Ac [m]	q [l/m/s]
V01	1.91	1.17	4.20	1.91	1.46	1.46	7.656
V02	1	1.17	4.20	1	1.46	1.46	
V03	2.17	1.17	4.20	2.17	1.46	1.46	6.933
V04	1.91	1.17	4.20	1.91	1.46	1.46	7.656
V05	2.8	1.20	4.34	2.8	1.4	1.4	7.754
V06	2.8	1.20	4.34	2.8	1.4	1.4	7.754
V07	2.2	1.20	4.34	2.2	1.67	1.67	5.252
V08	2.2	1.20	4.34	2.2	1.67	1.67	5.252
V09	2.2	1.20	4.34	2.2	1.67	1.67	5.252
V10	2.2	1.20	4.34	2.2	1.6	1.6	4.694
V11	2.2	1.20	4.34	2.2	1.6	1.6	4.694
V12	2.2	1.20	4.34	2.2	1.6	1.6	4.694
V13	2.2	1.20	4.34	2.2	1.6	1.6	4.694
V14	2.2	1.20	4.34	2.2	1.6	1.6	4.694
V15	2.2	1.20	4.34	2.2	1.67	1.67	5.252
V16	2.2	1.20	4.34	2.2	1.67	1.67	5.252
V17	2.2	1.20	4.34	2.2	1.15	1.15	5.722
V18	1.1	1.17	4.20	1.1	1.22	1.22	21.4
V19	2.46	1.13	3.52	2.46	1.65	1.65	2.692
V20	3.35	1.17	4.20	3.35	1.65	1.65	4.069

(Cont.on next page)

Table 7.1. (Cont.)

V21	3.18	1.43	4.41	3.18	1.4	1.4	15.82
V22	0.63	1.43	4.41	0.63	1.46	1.46	
V23	0.6	1.43	4.41	0.6	1.46	1.46	
V24	0.6	1.43	4.41	0.6	1.46	1.46	
V25	0.6	1.43	4.41	0.6	1.46	1.46	
V26	0.6	1.43	4.41	0.6	1.46	1.46	
V27	0.6	1.43	4.41	0.6	1.46	1.46	
V28	1.2	1.46	3.78	1.2	1.9	1.9	
V29	2.43	1.17	4.20	2.43	1.15	1.15	12.94
V30	2.43	1.17	4.20	2.43	1.2	1.2	11.49
V31	2.42	1.17	4.20	2.42	1.2	1.2	11.52
V32	2.46	1.17	4.20	2.46	1.12	1.12	13.73
V33	2.43	1.17	4.20	2.43	1.2	1.2	11.49
V34	2.42	1.17	4.20	2.42	1.2	1.2	11.52
V35	2.42	1.17	4.20	2.42	1.33	1.33	8.539
V36	2.42	1.17	4.20	2.42	1.95	1.95	0.7931
V37	2.42	1.17	4.20	2.42	1.15	1.15	12.97
V38	2.42	1.17	4.20	2.42	1.15	1.15	12.97
C1	2.35	1.43	4.41	2.35	1.3	1.3	22.65
C2	2.1	1.43	4.41	2.1	1.3	1.3	24.21
C3	1.85	1.43	4.41	1.85	1.25	1.25	28.69
C4	2	1.43	4.41	2	1.15	1.15	33.36
C5	2.3	1.43	4.41	2.3	1.2	1.2	28.15
C6	1.8	1.43	4.41	1.8	1.27	1.27	28.04
C7	1.25	1.43	4.41	1.25	1.3	1.3	30.93

In order to decide that these calculated discharges are dangerous for the people and the vehicles, tolerable limits should be known. Table 7.2 gives the tolerable overtopping discharge limits for people and vehicles behind vertical coastal protection structures (EurOtop, 2018).

Table 7.2. Limits for overtopping for people and vehicles

Hazard type and reason	**Mean discharge q (l/s per m)**
People at structures with possible violent overtopping, mostly vertical structures	No access for any predicted overtopping
People at seawall/dike crest. Clear view of the sea. Hm0 = 3 m Hm0 = 2 m Hm0 = 1 m Hm0 < 0.5 m	 0.3 1 10-20 No limit

(Cont.on next page)

Table 7.2. (Cont.)

Cars on seawall / dike crest, or railway close behind crest Hm0 = 3 m Hm0 = 2 m Hm0 = 1 m	 <5 10-20 <75
Highways and roads, fast traffic	Close before debris in spray becomes dangerous

Considering the calculated overtopping discharges in Table 7.1 and tolerable limits given in Table 7.2, it can be stated that 17 vertical sea wall sections (colored in Table 7.1) are above the tolerable limit. Table 7.3. shows the results of the overtopping discharges in case of the water level rise by 1 m during the storm in the future. Here, the water depth has been increased by 1m and the Rc (crest freeboard relative to SWL) and Ac (armor freeboard relative to SWL) values have been decreased by 1m. When Rc and Ac are below the limit value, the limit value is used for Rc and Ac values. However, if the water depth (h) remained below the limit, the calculation was not performed.

Table 7.3. Input parameters and calculated overtopping discharge for vertical walls at 1 m increased water level

Name	h [m]	Hm0 [m]	Tm-1.0 [s]	ht [m]	Rc [m]	Ac [m]	q [l/m/s]
V01	2.91	1.17	4.20	2.91	0.59	0.59	49.34
V02	2.00	1.17	4.20	2.00	0.59	0.59	56.14
V03	3.17	1.17	4.20	3.17	0.59	0.59	48.52
V04	2.91	1.17	4.20	2.91	0.59	0.59	49.34
V05	3.80	1.20	4.34	3.80	0.60	0.60	50.35
V06	3.80	1.20	4.34	3.80	0.60	0.60	50.35
V07	3.20	1.20	4.34	3.20	0.67	0.67	43.75
V08	3.20	1.20	4.34	3.20	0.67	0.67	43.75
V09	3.20	1.20	4.34	3.20	0.67	0.67	43.75
V10	3.20	1.20	4.34	3.20	0.60	0.60	43.75
V11	3.20	1.20	4.34	3.20	0.60	0.60	51.85
V12	3.20	1.20	4.34	3.20	0.60	0.60	51.85
V13	3.20	1.20	4.34	3.20	0.60	0.60	51.85
V14	3.20	1.20	4.34	3.20	0.60	0.60	51.85
V15	3.20	1.20	4.34	3.20	0.67	0.67	43.75
V16	3.20	1.20	4.34	3.20	0.67	0.67	43.75

(Cont. on next page)

Table 7.3. (Cont.)

V17	3.20	1.20	4.34	3.20	0.60	0.60	51.85
V18	2.10	1.17	4.20	2.10	0.59	0.59	54.93
V19	3.46	1.13	3.52	3.46	0.65	0.65	32.44
V20	4.35	1.17	4.20	4.35	0.65	0.65	39.56
V21	4.18	1.43	4.41	4.18	0.72	0.72	62.81
V22	1.63	1.43	4.41	1.63	0.72	0.72	84.25
V23	1.60	1.43	4.41	1.60	0.72	0.72	84.89
V24	1.60	1.43	4.41	1.60	0.72	0.72	84.89
V25	1.60	1.43	4.41	1.60	0.72	0.72	84.89
V26	1.60	1.43	4.41	1.60	0.72	0.72	84.89
V27	1.60	1.43	4.41	1.60	0.72	0.72	84.89
V28	2.20	1.46	3.78	2.20	0.90	0.90	42.21
V29	3.43	1.17	4.20	3.43	0.59	0.59	47.93
V30	3.43	1.17	4.20	3.43	0.59	0.59	47.93
V31	3.42	1.17	4.20	3.42	0.59	0.59	47.95
V32	3.46	1.17	4.20	3.46	0.59	0.59	47.87
V33	3.43	1.17	4.20	3.43	0.59	0.59	47.93
V34	3.42	1.17	4.20	3.42	0.59	0.59	47.95
V35	3.42	1.17	4.20	3.42	0.59	0.59	47.95
V36	3.42	1.17	4.20	3.42	0.95	0.95	47.95
V37	3.42	1.17	4.20	3.42	0.59	0.59	47.95
V38	3.42	1.17	4.20	3.42	0.59	0.59	47.95
C1	3.35	1.43	4.41	3.35	0.72	0.72	64.65
C2	3.10	1.43	4.41	3.10	0.72	0.72	65.7
C3	2.85	1.43	4.41	2.85	0.72	0.72	67.17
C4	3.00	1.43	4.41	3.00	0.72	0.72	66.23
C5	3.30	1.43	4.41	3.30	0.72	0.72	64.84
C6	2.80	1.43	4.41	2.80	0.72	0.72	67.53
C7	2.25	1.43	4.41	2.25	0.72	0.72	73.33

As seen in Table 7.3, when the water level increased 1m, the overtopping tolerable discharge limit are exceeded in all sections.

7.2. Overtopping Discharge Results for Rubble Mound Sloping Structures

Table 7.4 shows the acceptable overtopping for rubble mound breakwaters. Therefore, the tolerable overtopping discharge limit is accepted as 1 m/l/s in this study.

Table 7.4. Overtopping discharge limit for Rubble mound breakwaters (EurOtop, 2018)

Hazard type and reason	**Mean discharge q (l/s per m)**
Rubble mound breakwaters; Hm0 > 5 m; no damage	1
Rubble mound breakwaters; Hm0 > 5 m; rear side designed for wave overtopping	5-10

In this study, 6 parameters for rubble mound sloped structure were kept the same and 9 parameters were changed according to the section dimensions and location. Parameters that are the same for all sections are β=0, Bt=0, γf=0.5 (0.4-0.6 for rock), B=0, hb=0, tan αB=0.Input values for rubble mound sloped structure at current still water level and the calculated overtopping discharge are given in Table 7.5. Here, the wave height and wave period are taken from Table 6.2. according to the section location.

Table 7.5. Input parameters and calculated overtopping discharge for rubble mound sloped structure at current still water level

Name	h [m]	Hm0 [m]	Tm-1 [s]	ht [m]	cot α d [-]	cot α u [-]	Rc [m]	Ac [m]	Gc [m]	q [l/m/s]
S01	0.8	1.2	4.34	0.8	2.91	2.91	1.06	1.02	4.86	
S02	2	1.2	4.34	2	2	2	1.1	1.1	4.85	0.1
S03	2	1.2	4.34	2	2	2	1.1	1.1	4.85	0.1
S04	1.95	1.2	4.34	1.95	2	2	1.15	1.15	4.85	0.08
S05	1.9	1.2	4.34	1.9	2	2	1.22	1.22	4.85	0.06
S06	2	1.2	4.34	2	2	2	1.37	1.1	4.85	0.07
S07	2	1.2	4.34	2	2	2	1.37	1.1	4.85	0.07
S08	2	1.2	4.34	2	2	2	1.37	1.1	4.85	0.07
S09	2	1.2	4.34	2	2	2	1.25	1.1	4.85	0.08
S10	0.3	1.13	3.51	0.3	2	2	2	2	2.75	
S11	0.35	1.13	3.51	0.35	2	2	1.95	1.95	3.84	
S12	0.3	1.13	3.51	0.3	2	2	1.5	1.5	3.84	
S13	0.3	1.13	3.51	0.3	2	2	1.5	1.5	3.74	
S14	0.3	1.13	3.51	0.3	2	2	1.5	1.5	3.83	
S15	0.3	1.13	3.51	0.3	2	2	1.5	1.5	3.85	
S16	0.3	1.13	3.51	0.3	2	2	1.5	1.5	3.65	
S17	2.4	1.43	4.41	2.4	2	2	1.5	1.5	3.85	0.13
S18	2.4	1.43	4.41	2.4	2	2	1.5	1.5	5.32	0.07
S21	1.5	1.43	4.41	1.5	2.35	2.35	1.4	0.92	3.84	0.33
S22	2	1.2	4.34	2	1.96	1.96	1.06	0.74	1.25	0.62
S23	1.3	1.2	4.34	1.3	1.96	1.96	1.7	1.4	1.4	0.25
S24	2	1.43	4.41	2	2	2	1.65	1.65	3.85	0.07

(Cont. on next page)

Table 7.5. (Cont.)

S25	2	1.13	3.51	2	2	2	1.65	1.65	3.85	0.01
S26	2.37	1.13	3.51	2.37	5.67	5.67	1.65	1.65	3.7	0.01
D-1	1.47	0.74	3.4	1.47	2	2	0.6	0.6	3.91	0.05
D-2	1.71	0.74	3.4	1.71	2	2	0.6	0.6	3.82	0.06
D-5	1.59	0.74	3.4	1.59	2	2	0.6	0.6	3.82	0.05
D-7	1.74	0.74	3.4	1.74	2	2	0.6	0.6	3.82	0.06
D-8	1.5	0.74	3.4	1.5	2	2	0.6	0.6	3.82	0.05
D-9	1.53	0.74	3.4	1.53	2	2	0.6	0.6	3.82	0.05
D-10	1.61	0.74	3.4	1.61	2	2	0.6	0.6	3.82	0.05
D-11	2.42	0.74	3.4	2.42	2	2	0.6	0.6	3.82	0.12
D-12	2.08	0.74	3.4	2.08	2	2	0.6	0.6	3.82	0.09
D-13	1.63	0.74	3.4	1.63	2	2	1.1	1.1	1.91	0.01
D-14	1.51	0.74	3.4	1.51	2	2	1.1	1.1	1.91	0.01
D-15	1.4	0.74	3.4	1.4	2	2	0.6	0.6	3.82	0.05
D-16	1.68	0.74	3.4	1.68	2	2	0.6	0.6	3.82	0.06
D-17	1.39	0.74	3.4	1.39	2	2	0.6	0.6	7.4	0.01
D-18	1.7	0.74	3.4	1.7	2	2	0.6	0.6	3.82	0.06
D-19	1.49	0.74	3.4	1.49	2	2	0.6	0.6	3.82	0.05
D-20	1.41	0.74	3.4	1.41	2	2	0.6	0.6	3.82	0.05
D-21	1.44	0.74	3.4	1.44	2	2	0.6	0.6	3.82	0.05

In the overtopping analysis for the rubble mound sloped structure at the still water level, no section discharge value was above the tolerable limit. Table 7.6. shows the results of the overtopping analysis made considering that the water level rose by 1 m during the storm. Here, the water depth has been increased by 1m and the Rc and Ac values have been decreased by 1m. Accordingly, when Rc and Ac are below the limit value, the limit value is used for Rc and Ac values. However, if the water depth (h) remained below the limit, the calculation was not made.

Table 7.6. Input parameters and calculated overtopping discharge for Rubble Mound Sloped Structure at 1 m increased water level

Name	h [m]	Hm0 [m]	Tm-1.0 [s]	ht [m]	cot α d [-]	cot α u [-]	Rc [m]	Ac [m]	Gc [m]	q [l/m/s]
S01	1.8	1.2	4.34	1.8	2.91	2.91	0.6	0.6	4.86	0.36
S02	3	1.2	4.34	3	2	2	0.6	0.6	4.85	1.17
S03	3	1.2	4.34	3	2	2	0.6	0.6	4.85	1.17
S04	2.95	1.2	4.34	2.95	2	2	0.6	0.6	4.85	1.13
S05	2.9	1.2	4.34	2.9	2	2	0.6	0.6	4.85	1.08
S06	3	1.2	4.34	3	2	2	0.6	0.6	4.85	1.17
S07	3	1.2	4.34	3	2	2	0.6	0.6	4.85	1.17

(Cont. on next page)

Table 7.6. (Cont.)

S08	3	1.2	4.34	3	2	2	0.6	0.6	4.85	1.17
S09	3	1.2	4.34	3	2	2	0.6	0.6	4.85	1.17
S10	1.3	1.13	3.51	1.3	2	2	1	1	2.75	0.15
S11	1.35	1.13	3.51	1.35	2	2	0.95	0.95	3.84	0.09
S12	1.3	1.13	3.51	1.3	2	2	0.56	0.56	3.84	0.49
S13	1.3	1.13	3.51	1.3	2	2	0.56	0.56	3.74	0.53
S14	1.3	1.13	3.51	1.3	2	2	0.56	0.56	3.83	0.49
S15	1.3	1.13	3.51	1.3	2	2	0.56	0.56	3.85	0.49
S16	1.3	1.13	3.51	1.3	2	2	0.56	0.56	3.65	0.57
S17	3.4	1.43	4.41	3.4	2	2	0.72	0.72	3.85	4.48
S18	3.4	1.43	4.41	3.4	2	2	0.72	0.72	5.32	1.51
S21	2.5	1.43	4.41	2.5	2.35	2.35	0.72	0.72	3.84	1.92
S22	3	1.2	4.34	3	1.96	1.96	0.6	0.6	1.25	22.39
S23	2.3	1.2	4.34	2.3	1.96	1.96	0.7	0.7	1.4	10.63
S24	3	1.43	4.41	3	2	2	0.72	0.72	3.85	3.4
S25	3	1.43	4.41	3	2	2	0.72	0.72	3.85	3.4
S26	3.37	1.43	4.41	3.37	5.67	5.67	0.72	0.72	3.7	0.41
D-1	2.47	0.74	3.4	2.47	2	2	0.37	0.37	3.91	0.42
D-2	2.71	0.74	3.4	2.71	2	2	0.37	0.37	3.82	0.57
D-5	2.59	0.74	3.4	2.59	2	2	0.37	0.37	3.82	0.52
D-7	2.74	0.74	3.4	2.74	2	2	0.37	0.37	3.82	0.56
D-8	2.5	0.74	3.4	2.5	2	2	0.37	0.37	3.82	0.45
D-9	2.53	0.74	3.4	2.53	2	2	0.37	0.37	3.82	0.47
D-10	2.61	0.74	3.4	2.61	2	2	0.37	0.37	3.82	0.5
D-11	3.42	0.74	3.4	3.42	2	2	0.37	0.37	3.82	0.98
D-12	3.08	0.74	3.4	3.08	2	2	0.37	0.37	3.82	0.77
D-13	2.63	0.74	3.4	2.63	2	2	0.37	0.37	1.91	4.32
D-14	2.51	0.74	3.4	2.51	2	2	0.37	0.37	1.91	4.16
D-15	2.4	0.74	3.4	2.4	2	2	0.37	0.37	3.82	0.43
D-16	2.68	0.74	3.4	2.68	2	2	0.37	0.37	3.82	0.56
D-17	2.39	0.74	3.4	2.39	2	2	0.37	0.37	7.4	0.05
D-18	2.7	0.74	3.4	2.7	2	2	0.37	0.37	3.82	0.57
D-19	2.49	0.74	3.4	2.49	2	2	0.37	0.37	3.82	0.47
D-20	2.41	0.74	3.4	2.41	2	2	0.37	0.37	3.82	0.44
D-21	2.44	0.74	3.4	2.44	2	2	0.37	0.37	3.82	0.45

As can be seen in Table 7.6, when the water level rises by 1 m, the overtopping discharge limit has been exceeded in 17 sections. Compared to vertical structures, the vulnerability of the rubble mound sloped structures to the wave overtopping is lower. Therefore, more attention should be taken for vertical structures considering the wave overtopping and the coastal flood.

CHAPTER 8

CONCLUSIONS

In this thesis, the coastal flood problem in Izmir Bay is investigated including all elements of the problem such as the wind climate, sea level fluctuations, wave climate, and coastal flood calculations. Following conclusions are drawn:

ERA5 wind dataset which is one of the newest re-analysis data produced by ECMWF, is compatible with the in-situ measured data in Foca especially for the higher wind speeds. Therefore, ERA5 dataset is convenient when the longer data set is necessary for example in the determination of design winds with the extreme value analysis.

Daily and seasonal tides, storm surge and barometric surge are analyzed using in-situ sea water level measurement data. It is seen that the mean water level is changing between (-60) cm to 76 cm. Negative values are due to negative amplitudes of daily and seasonal tides and positive values are due to storm and barometric surges in addition to positive amplitudes of daily and seasonal tides.

When the trend analysis is performed with normalized sea water levels obtained from the mareograph station at TUDES Mentes location, it is observed that the sea water level is increasing. When the trend is examined with Theil-Sen and the line of best fit techniques, an increase is observed in all months and as annual. Trends and their reliability are checked using Mann-Kendall test. Mann-Kendall test show that the calculated increasing trends for the mean water level and the maximum water level are reliable. However, while Theil-Sen and the line of best fit method gave increasing trend for January and November, Mann-Kendall estimated a decreasing trend. The annual increase rate of sea water level is 0.284 %/year and 0.306 %/year according to Theil-Sen estimator and the line of best fit method, respectively. It means that if the water depth is 2m, it may rise 28.4% in 100 years and reach to 2.57m and 2.61m according to Theil-Sen and the line of best fit estimation methods, respectively.

Wave heights and periods are estimated using SWAN numerical wave model. The wave heights with 100 yrs return periods are determined at the critical areas along the Izmir inner bay. The maximum significant wave height is observed at Konak region with Hs=1.4m and Tp=4.8 s.

In order to determine the effect of coastal flooding, wave overtopping amounts on the coastal protection structures are calculated. Neural Network model developed by the Deltares team is used to calculate the overtopping discharges. Overtopping discharges are calculated for almost 90 cross-sections of the structures along the Izmir Bay for the current sea water level (0.0) and high water level, HWL (+1.0m) cases. Coastal protection structures in Izmir Bay include vertical walls and sloping type rubble mound revetments. Calculated overtopping discharges are compared with the tolerable limits and it is seen that especially vertical wall structures are not efficient against wave overtopping and coastal flooding. In the case of HWL, some sloping type revetment cross-sections also allow higher overtopping values.

Coastal flood amounts calculated in this study and the increase in the coastal flood events show that it is compulsory to develop mitigation solutions to prevent the coastal flood hazard in İzmir Bay. To propose solutions is a future study. It should be noted here that the proposed solutions should be examined under numerical and physical models before applying them at the site.

REFERENCES

Aydoğan, B., & Ayat, B. (2018). Spatial variability of long-term trends of significant wave heights in the Black Sea. Applied Ocean Research, 79(July), 20–35. https://doi.org/10.1016/j.apor.2018.07.001

Battjes, J. A., & Janssen, H. (1978). Energy Loss and Set-Up Due to Breaking of Random Waves. Coastal Engineering Proceedings, 1, 32. https://doi.org/10.9753/icce.v16.32

Besiktepe, S., Sayin, E., İlhan, T., & Tokat, E. (2011). İzmir Körfezi Akıntı Dinamiğinin Model ve Gözlem Yardımıyla İncelenmesi.

Bilyay, E., Ozbahceci, B., & Yalciner, A. (2011). Extreme waves at Filyos, Southern Black Sea. Natural Hazards and Earth System Sciences - NAT HAZARDS EARTH SYST SCI, 11, 659–666. https://doi.org/10.5194/nhess-11-659-2011

Collins, M., Sutherland, M., Bouwer, L., Cheong, S.-M., Frölicher, T. L., Jacot Des Combes, H., Roxy, M. K., Losada, I., McInnes, K., Ratter, B., Rivera-Arriaga, E., Susanto, R. D., Swingedouw, D., Tibig, L., Bakker, P., Eakin, C. M., Emanuel, K., Grose, M., Hemer, M., … Timmermans, M.-L. (2019). Extremes, Abrupt Changes and Managing Risks: IPCC Special Report on the Ocean and Cryosphere in a Changing Climate. IPCC Special Report on the Ocean and Cryosphere in a Changing Climate, 589–655. https://report.ipcc.ch/srocc/pdf/SROCC_FinalDraft_Chapter6.pdf

Demirkesen, A. C., Evrendilek, F., Berberoglu, S., & Kilic, S. (2007). Coastal flood risk analysis using landsat-7 ETM+ imagery and SRTM DEM: A case study of Izmir, Turkey. Environmental Monitoring and Assessment, 131(1–3), 293–300. https://doi.org/10.1007/s10661-006-9476-2

ECMWF. ERA 5. Retrieved from https://www.ecmwf.int/en/forecasts/datasets/reanalysis-datasets/era5.

El-Shaarawi, Abdel H.; Piegorsch, Walter W. (2001). Encyclopedia of Environmetrics, Volume 1, John Wiley and Sons, p. 19, ISBN 978-0-471-89997-6.

Ergin, A., & Guler, I. (2014). Impacts of Climate Change on Coastal Structures and Planning of Coastal Cities. İzmir Su Sempozyumu

EurOtop (2018). Manual on wave overtopping of sea defenses and related structures, an overtopping manual largely based on European research, but for worldwide application, Second Edition 2018, http://www.overtopping-manual.com/

Goda, Y. (2000) Random Seas and Design of Maritime Structures. World Scientific, Singapore. http://dx.doi.org/10.1142/3587

Goda, Y. (2010). Random seas and design of maritime structures. Advanced series on ocean engineering: Vol. 33, 3rd ed. World Scientific Publishing Co. Pte. Ltd.

Guérin, T., Bertin, X., Coulombier, T., & de Bakker, A. (2018). Impacts of wave-induced circulation in the surf zone on wave setup. Ocean Modelling, 123(July 2017), 86–97. https://doi.org/10.1016/j.ocemod.2018.01.006

Hasselmann, K., Barnett, T. P., Bouws, E., Carlson, H., Cartwright, D., Enke, K., Ewing, J. A., Gienapp, H., Hasselmann, D., Kruseman, P., Meerburg, A., Muller, P., Olbers, D., Richren, K., Sell, W., & Walden, H. (1973). Measurements of wind-wave growth and swell decay during the Joint North Sea Wave Project (JONSWAP). 1–95.

Hersbach, H. et al. (2020). The ERA5 Global Reanalysis. Quarterly Journal of the Royal Meteorological Society, 146, 1999-2049. https://doi.org/10.1002/qj.3803

https://earth.esa.int/web/earth-watching/image-of-the-week/content/-/article/izmir-turkey/index.html

Kamphius, J.W. (2020). Introduction to Coastal Engineering and Management. Advanced Series on Ocean Engineering: Volume 48, World Scientific,3rd Edition.

Karaca, M., & Nicholls, R. (2008). Potential Implications of Accelerated Sea-Level Rise for Turkey. Journal of Coastal Research - J COASTAL RES, 24, 288–298. https://doi.org/10.2112/07A-0003.1

Kisacik, D., Ozyurt Tarakcioglu, G., Baykal, C., Keles, B., Kaboğlu, G., & Güler, I. (2016). Storm Surge and Flooding in Izmir Bay and a Suggestion for Coastal Protection Stilling Wave Basin.

NOAA (1998). Our Restless Tides. A Brief Explanation Of The Basic Astronomical Factors Which Produce Tides And Tidal Currents. http://140.90.121.76/restles1.html

Ozbahceci, B., & Bilyay, E. (2018). Effect of the armor crest freeboard relative to the crown wall freeboard on wave overtopping for simple rubble mound slopes. Ocean Engineering, 169, 511–528.

Ozbahceci, B. (2019). Extreme Value Statistics of Wind Speed and Wave Height of the Marmara Sea Based on Combined Radar Altimeter Data. Advances in Space Research, 66. https://doi.org/10.1016/j.asr.2019.08.025

Ozbahceci, B., Turgut, A., Bozoklu, A., & Abdalla, S. (2020). Calibration and Verification of Century Based Wave Climate Data Record along the Turkish Coasts Using Satellite Altimeter Data. Advances in Space Research, 66. https://doi.org/10.1016/j.asr.2020.02.021

OCDI (2009) Technical Standards and Commentaries for Port and Harbour Facilities in Japan. OCDI, Japan.

Pugh, D. (2004). Changing Sea Levels. Effects of Tides, Weather and Climate, Southampton Oceanography Centre, UK.

Steendam, G.J., J.W. van der Meer, H. Verhaeghe, P. Besley, L. Franco and M.R.A. van Gent (2004), The international database on wave overtopping, World Scientific, Proc. 29th ICCE, Vol.4, 4301-4313, https://doi.org/10.1142/9789812701916_0347

SWAN team (2017). SWAN Scientific and Technical Documentation. SWAN Cycle III version 41.20 Delft University of Technology, Netherlands.

Van Gent, M.R.A., H.F.P. van den Boogaard, B. Pozueta and J.R. Medina (2007). Neural network modelling of wave overtopping at coastal structures, Elsevier, Coastal Engineering, 54, 586-593, https://doi.org/10.1016/j.coastaleng.2006.12.001

Woodworth, P.L. (1987). Trends in U.K. Mean Sea Level", Marine Geodesy, Vol.11, pp. 57-87.

Yue, S., Pilon, P., Cavadias, G. (2002). Power of The Mann-Kendall and Spearman's Rho Tests For Detecting Monotonic Trends in Hydrological Series, Journal of Hydrology 259: 254-271.

Zhang, X., Harvey, K.D., Hogg, W.D., Yuzyk, T.R. (2001). Trends in Canadian Streamflow, Water Resources Research 37 (4): 987-998.

Zijlema, M., Vledder, G., & Holthuijsen, L. (2012). Bottom friction and wind drag for wave models. Coastal Engineering, 65, 19–26. https://doi.org/10.1016/j.coastaleng.2012.03.002